Aus der Klinik für Unfallchirurgie, Orthopädie und Plastische Chirurgie

(Prof. Dr. med. W. Lehmann)

der Medizinischen Fakultät der Universität Göttingen

Cell-cell communication between chondrocytes and osteoblasts through miR-221-3p loaded extracellular vesicles

INAUGURAL-DISSERTATION

zur Erlangung des Doktorgrades

der Medizinischen Fakultät der

Georg-August-Universität zu Göttingen

vorgelegt von

Xiaobin Shang

aus

Shangqiu, Henan, China

Göttingen 2022

Dekan: Prof. Dr. med. W. Brück

Betreuungsausschuss

Betreuer/in: Prof. Dr. med. A. Schilling

Ko-Betreuer/in: Prof. Dr. N. Miosge

Prüfungskommission

Referent/in: Prof. Dr. med. A. Schilling

Ko-Referent/in: PD Dr. Dr. Phillipp Brockmeyer

Drittreferent/in:

Datum der mündlichen Prüfung: 2022-09-15

Hiermit erkläre ich, die Dissertation mit dem Titel "Cell-cell communication between chondrocytes and osteoblasts through miR-221-3p loaded extracellular vesicles" eigenständig angefertigt und keine anderen als die von mir angegebenen Quellen und Hilfsmittel verwendet zu haben.

Göttingen, den 2022-08-17 Xiaobin Shang

(Unterschrift)

TABLE OF CONTENTS

LIST OF FIGURES

LIST OF FIGURES

LIST OF TABLES

ABBREVIATIONS

ACC	Articular cartilage chondrocyte
ADAMTS5	A disintegrin, and metalloproteinase with thrombospondin motifs 5
AGG	Aggrecan
Alix	ALG2 interacting protein X
ARNT	Aryl hydrocarbon receptor nuclear translocator
ARNT	Mesenchymal stem cells
BM	Basic medium
COL1A1	Collagen Type I Alpha 1 Chain
COL1	Collagen I
COL2A1	Collagen Type II Alpha 1 Chain
COL2	Collagen II
COX2	Cyclooxygenase 2
CPC	Chondrogenic progenitor cell
CXCR4	C-X-C chemokine receptor type 4
DAPI	4',6-diamidino-2-phenylindole
Dexa	Dexamethasone
DMEM	Dulbecco's Modified Eagle Medium
DNA	deoxyribonucleic acid
DPBS	Dulbecco's phosphate-buffered saline
ECL	electrogenerated chemiluminescence
ECM	Extra cellular matrix
EV	Extracellular vesicles
FBS	Fetal Bovine Serum
GAPDH	Glycerinaldehyd-3-phosphat-Dehydrogenase
GWAS	Genome-wide association study
HDAC	Histone deacetylase inhibitors
IL-1β	Interleukin 1 beta
ILVs	Intraluminal vesicles
MiRNA	MicroRNA
MMP13	Matrix metallopeptidase 13

MMP2	Matrix metalloproteinase 2
MRI	Magnetic Resonance Imaging
MSC	Mesenchymal stem cell
MVBs	Multivesicular bodies
MVs	Microvesicles
NSAIDs	Non-steroidal anti-inflammatory drugs
NTA	Nano-track analysis
OA	Osteoarthritis
OB	Osteoblast
OCN	Osteocalcin
ODM	Osteogenic differentiation medium
P/S	Penicillin/Streptomycin
CDKN1B/p27	Cyclin-dependent kinase inhibitor 1B
PBS	Phosphate-buffered saline
PEG	Polyethylene glycol
PRP	Platelet-rich plasma
PVDF	Polyvinylidene fluoride or polyvinylidene difluoride
qRT-PCR	Real-Time Quantitative Reverse Transcription PCR
RIPA	Radioimmunoprecipitation assay
RISC	RNA-induced silencing complex
RNA	Ribonucleic Acid
RUNX2	Runt-related transcription factor 2
SDF1	Stromal cell-derived factor 1
SDS-PAGE	SDS-polyacrylamide gel electrophoresis
SOX9	Transcription factor SOX9
TBS-T	Tris-buffered saline with 0.1% Tween® 20 detergent
Tcf7l2/TCF4	Transcription factor 7-like 2
TGFβ	Transforming growth factor beta
TIMP3	TIMP Metallopeptidase Inhibitor 3
TSG101	Tumor susceptibility Gene 101
U6	U6 small nuclear RNA

VEGF	Vascular endothelial growth factor
YLDs	Years lived with disability

ABSTRACT

Osteoarthritis (OA) is a whole joint disease manifested by cartilage degeneration and subchondral bone remodeling, and bone-cartilage communication plays a vital role in the disease progression with the existence of microchannels across the bone-cartilage interface. However, the knowledge of how the signal transduction from chondrocytes to osteoblasts happens is limited. Recently, *miR-221-3p* was demonstrated to be mechanosensitive in cartilage chondrocytes and extracellular vesicles (EVs) have been deeply researched for a specific role in cell-cell communication. In the present study, we investigated the role of EVs in chondrocyte-osteoblast communication by transferring the signal of *miR-221-3p*. EVs were isolated from the supernatant of chondrocytes by the PEG precipitation method and identified with nanoparticle tracking analysis (NTA) and western blot. The results suggest that the chondrocytes secreted EVs not only mediate the communication of these two cells in a coculture model but also inhibit the bone formation capacity of osteoblasts via the cargo of *miR-221-3p*. Therefore, this study provides a novel perspective on the communication between chondrocytes and osteoblasts through EVs and this can be considered a reliable approach to modulate the bone-cartilage remodeling in the future.

1. Introduction

1.1. Osteoarthritis

Osteoarthritis (OA) is a chronic disease that preferentially damages weight-bearing joints and affects patients all over the world. OA can cause serious consequences for its pain-induced disability and the morbidity is rising due to the aged tendency of the population globally (Nelson 2018). Furthermore, what was previously a disease of the elderly is becoming common among young people owing to a sedentary lifestyle and obesity (Cross et al. 2014). According to one research study conducted in 2017, more than three million patients are affected with symptomatic OA (GBD 2017). With the increasing number of patients, OA also causes a serious socioeconomic burden. It has been estimated that only in the USA, the direct costs and loss of earnings caused by OA each year increased from $128billion in 2003 to $304billion in 2013 (Yelin et al. 2007; Murphy et al. 2018). Although OA could affect any moving joints, such as knees, hips, hands, temporomandibular joint, and spinal facet joints, knee joint OA accounts for 83% of the total OA burden based on the years lived with disability (YLDs), an indicator to evaluate the impact of non-fatal diseases and injuries (Vos et al. 2012). As one of the largest and most flexible weight-bearing joints in the human body, knee joints are prone to get injured and develop osteoarthritis caused by aging and wear-tear of cartilage which plays a crucial role in maintaining the normal function of the knee joint in daily activities. In addition to articular cartilage, other structures making up the knee joint are involved in the occurrence and progression of OA. More details of the pathogenesis of OA are provided in the following chapter (1.3). The most common clinical symptoms of OA include early clinical manifestations such as pain, swelling, and stiffness, while deformity and disability in the end-stage. Despite years of research, there is still no effective treatment to stop or reverse the pathological progression of OA. Until now, almost all treatment regimens can only relieve clinical symptoms. As a result, it is urgent to find new and effective treatment methods to save OA patients' joints.

1.2. Etiology

Knee joint osteoarthritis can be classified into two categories including primary and secondary forms according to specific reasons causing OA. Compared with primary OA which is an idiopathic phenomenon caused by the aging process and mainly occurs in older patients, secondary OA is always with initiating factors and commonly happens in young

people, for example, traumatic osteoarthritis. Primary OA is possible due to early or insignificant microdamage and there is no essential difference between these two entities. Both the primary and secondary OA primarily initiate in the degraded articular cartilage which could be caused by either excessive mechanical stress on a healthy joint or normal loading on an injured joint (Madry et al. 2016). It has been demonstrated OA progress can be affected by many different risk factors such as age, sex, trauma, obesity, and genetic predisposition, all of which can also be vital therapeutic targets. It is easy to understand how aging reduces articular cartilage volume and quality, then destroys the normal function to dispersive mechanical loading, thus leading to the occurrence of OA (Rahmati et al. 2017). Although age is not a necessary condition for the development of OA, studies have demonstrated a significant increase in the morbidity of OA along with age (Cross et al. 2014; Spitaels et al. 2020). Sex could affect the initiation and progression of knee joint osteoarthritis, in females versus males, while the specific reasons are elusive (O'Connor 2006). Previous studies have found gender-specific anatomy and kinematics in the knee joint and there are significant differences in endocrine hormone levels between different genders. The gender-specific factors could help us better understand the clinical symptom in female patients and choose specific treatment considering women's representation in scientific research which lags behind that of men's (Ramasubbu et al. 2001). During the above risk factors, obesity may play a special role in the pathogenesis of OA, not only for the adverse mechanical stress but also for the inflammation in adipose tissue. More details of the pathogenesis of OA attributable to obesity are provided in the next chapter (1.3). As for the trauma, even microdamage in daily life such as squatting, stair-climbing, or kneeling may induce OA. What's more, compared with the damage caused by excessive activity, lack of physical activity may also contribute to the increasing prevalence of OA owing to the weakness of extensor muscles around the knee joint (Hunter und Bierma-Zeinstra 2019). With larger numbers of genome-wide association studies (GWAS) on OA, our understanding of the genetic etiology of OA has been greatly enhanced. So far, scientists have identified nearly 100 genetic risk loci for OA (Zengini et al. 2018; Tachmazidou et al. 2019). The most important problem facing us today is how to associate genetic risk loci with the pathological progression of OA and translate genomic evidence into the development of disease-modifying therapies for osteoarthritis is still an issue and needs further research. Recent Studies found except for the genetic risk loci, epigenetic mechanisms such as DNA methylation, histone modification, and non-coding RNA may also participate in OA pathogenesis and progression, and even provide promising therapeutic targets (Rice et al. 2020).

1.3. Pathogenesis

Articular cartilage is a transparent, smooth, and elastic tissue without vessels and nerves, and is mainly comprised of extracellular matrix (ECM) and chondrocytes. In the past decades, OA was considered a disease of cartilage caused by the disbalance of catabolic and anabolic metabolism in the ECM and senescence or apoptosis of chondrocytes. Recently, it was found that structural changes of subchondral bone may be even in advance of cartilage degradation because the subchondral bone is much more sensitive in response to mechanical force-induced structural remodeling compared to a slower turnover rate of the articular cartilage (Zhen und Cao 2014). As a result, subchondral bone may play an initial role in the pathogenesis of OA. Meanwhile, the view is accepted that interaction between articular cartilage and subchondral bone is due to the existence of various microchannels in the interface of these two parts (Pan et al. 2009). The latest opinion considered OA as a whole joint disease instead of simple cartilage destruction. More importantly, all the tissues in or around the joint could contribute to the pathogenesis of OA. For example, synovium which could secret synovial fluid to provide nutrition for the avascular cartilage and lubricate joints to reduce friction in motion under normal circumstances can be a double-edged sword (Loeser et al. 2012). In clinical, it is common to meet OA patients whose main complaint is knee swelling and pain caused by thickened synovium which could secret inflammatory cytokines, also called synovitis, an early-stage feature of knee joint OA (Griffin und Scanzello 2019). Therefore, OA is now considered a low-grade inflammatory disease instead of pure wear and tear disease caused by abnormal mechanical loading. Other parts of the knee joint including meniscus, ligaments, tendons, muscles and infrapatellar fat pad also participate in the pathogenic process for their abnormal performance (Alnahdi et al. 2012; Heijink et al. 2012; van der Voet et al. 2017; Krishnasamy et al. 2018; Rothrauff et al. 2020). As mentioned before, obesity can be also an increasing risk factor for the development of OA. However, the exact mechanism of how obesity increases the risk of OA is elusive, and it is hard to believe that increased joint loading and metabolic factors could be the only explanation (Aspden 2011). It was demonstrated that obesity was associated with OA even in patients without a weight-bearing problem and patients can obtain better clinical outcomes by diet than exercise (Urban und Little 2018).

1.4. Treatment

Osteoarthritis is a chronic non-fatal disease that usually lasts for years, and most of the patients are elderly people with multimorbidities, such as cardiovascular and cerebrovascular diseases, endocrine diseases, respiratory diseases, and even psychological disorders caused by

limited activity, so the treatment options should be individualized. Since pain is the chief complaint in early patients, the primary therapeutic objective is to relieve pain by pharmacological and non-pharmacological methods to restore the normal function of the knee joint and delay the progression of the disease. For these patients, traditional drugs, like paracetamol, non-steroidal anti-inflammatory drugs (NSAIDs), corticosteroid injections, and tramadol are recommended according to recent guidelines (Nelson et al. 2014; Kolasinski et al. 2020). Although these treatments can relieve pain to a certain extent, their therapeutic effect is limited and always with some adverse effects. For example, a Cochrane review in 2019 found paracetamol provides only minimal improvements in pain and doesn't show a difference between different doses (Leopoldino et al. 2019). In addition to the gastrointestinal side effects, increased cardiovascular risk is another problem needed to be considered for NSAIDs, including COX2 selective or nonselective inhibitors (Zeng et al. 2018). Intraarticular corticosteroids in the knee joint should be strictly controlled because long-term use can damage the volume of cartilage based on MRI evidence (McAlindon et al. 2017). Tramadol, one of the so-called weak opioid analgesics, is often used to alleviate severe pain when paracetamol or NSAIDs have not been satisfactory in clinical work. But whether weak opioids are more effective than paracetamol or NSAIDs on nociceptive pain requires further research, considering its serious adverse effects (Schmid et al. 2017). Compared with pharmacological treatment, non-pharmacological management, such as exercise and physical therapy may be much safer and more suitable especially for obese patients and patients with multimorbidities. Of note, based on the conclusion of recent clinical trials and systematic reviews, exercise therapy demonstrates moderate positive benefits for symptomatic OA patients (Hurley et al. 2018). However, joint replacement is an effective therapeutic method for patients with end-stage OA, but joint replacement surgery has also its disadvantages such as high costs, infection, revision, and other problems (Bayliss et al. 2017). Recently, regenerative treatment such as mesenchymal stem cell (MSC), platelet-rich plasma (PRP), and related extracellular vesicles (EVs) has been tested to treat OA (Mora et al. 2018). These methods focused on the reduction of inflammation, and stimulation of anabolism and chondrogenic differentiation via growth factors, cytokines, and other means such as miRNAs. Although they are reported to be promising to relieve pain and reestablish knee joint homeostasis, further research is necessary to clarify the exact regulatory mechanisms.

1.5. MicroRNAs in OA

Micro ribonucleic acids (Short for miRNAs) are non-coding single-stranded RNAs (Lee et al. 1993). MicroRNAs are usually transcribed in the nucleus with the modulation of RNA polymerase II (Lee et al. 2004; Zhou et al. 2007). After a series process, the pre-miRNAs are then exported from the nucleus to the cytoplasm by Exportin 5 (Murchison und Hannon 2004). Once the pre-miRNAs are exported to the cytoplasm, the RNase III enzyme Dicer cleaves the pre-miRNA hairpin, which results in the generation of mature miRNA duplex (around 22 nucleotides) (Lund und Dahlberg 2006), one strand of which participate in the RNA-induced silencing complex (RISC) and interact with relevant mRNA targets (Rana 2007). MiRNA induced target inhibition may be achieved by mRNA degradation or by preventing mRNA from translation(Jing et al. 2005; Lim et al. 2005). More than 1900 miRNAs are encoded by the human genome and seem to modulate about 60% of the genes of humans (Friedman et al. 2009). Thus, changing the expression of miRNAs will impact a cascade of modifications in gene expression. However, it is still not easy to predict the specific action of miRNAs on their mRNA targets, because each miRNA has more than one mRNA target and vice versa; therefore, the correct identification of miRNA's targets remains a challenge even though prediction databases such as Public online websites including Targetscan, miRWalk, and miRDB are available so far. As a result, further research is essential to exploit miRNAs as a reliable treatment of OA (Riffo-Campos et al. 2016). During the past decades, many studies have reported the abnormal expression of miRNAs in OA patients. Computer analysis shows that miRNAs achieve the complex regulation in the homeostasis of articular cartilage by inhibiting various mRNA targets and modulating many different signaling pathways. As a result, miRNAs have been reported to be able to mediate protective or destructive effects on the therapeutic potential (Endisha et al. 2018). Although *miR-221-3p* is one of the miRNAs that regulate cell proliferation, invasion, and apoptosis in different fields, the role of *miR-221* in OA remains to be fully elucidated (Fu et al. 2015). Recently, *miR-221-3p* was reported to be able to inhibit IL-1β-mediated catabolic responses by targeting SDF1 and inhibiting the SDF1/CXCR4 pathway in human chondrocytes (Zheng et al. 2017). Another study demonstrated *miR-221-3p* can be mechanosensitive under anabolic and catabolic mechanical loading on human chondrocytes (Hecht et al. 2019). Based on the above evidence, *miR-221-3p* may play a vital role in the pathogenesis of OA by modulating inflammation and mechanotransduction. The latest research found exosomal *miR-221-3p* from chondrogenic progenitor cells (CPCs) may play a vital role in promoting cartilage regeneration and stimulating migration and proliferation of chondrocytes (Wang et al. 2020). According to the aforementioned, the presence of connections (microfractures,

fissures, vascular channels) between subchondral bone and cartilage could provide pathways of communication across the osteochondral interface (Taheri et al. 2021). Therefore, exosomal *miR-221-3p* may regulate the pathogenesis of OA through participation in the communication between chondrocytes in the cartilage and osteoblasts in the subchondral bone.

1.6. Extracellular vesicles and cell-cell communication

Extracellular vesicles (EVs) are nano-sized vesicles and can be synthesized and secreted by most cells *in vitro* and *in vivo* (Colombo et al. 2014). Although EVs were at first thought of as a kind of excrement to eliminate unwanted components from the cell, people came to realize that the function of extracellular vesicles was more than just waste carriers (Lo Cicero et al. 2015). What is more, these nano-sized vesicles may act as an important role in cell-cell communication by the trafficking of the specific cargoes, including nucleic acids (such as DNA, mRNA and miRNA), lipids, and proteins among different cells (Yáñez-Mó et al. 2015). With the understanding of the nano-sized vesicles, extracellular vesicles have gone through different kinds of nomenclatures in literature according to their size, origin, presence outside of cells, and their biogenesis, while the standard nomenclature is still controversial (Gould und Raposo 2013). However, with further research into the biogenesis of the nano-sized vesicles, especially by transmission electron microscopy and other biochemical methods, EVs can be mainly classified into three main subclasses: exosomes, microvesicles (MVs) and apoptotic vesicles. The typical size distribution of exosomes ranges from 30nm to 200 nm (Pegtel und Gould 2019). Exosomes are derived from intraluminal vesicles (ILVs) within the lumen of multivesicular bodies (MVBs) and then secreted outside during the fusion of MVBs with the plasma membrane (PM). The particle size of microvesicles ranges mainly from 50 nm to 1,000 nm in diameter. What's the difference in the biogenesis of MVs compared with exosomes is that MVs are generated by the outward budding and fission of the PM, thereafter released into the extracellular space. Apoptotic vesicles released from apoptotic cells, also called oncosomes in cancer cells are with a diameter ranging from 1000nm to 5000nm, sometimes even larger to 10 μm (Théry et al. 2001; Minciacchi et al. 2015). In fact, the size which was thought as a decisive factor to distinguish different vesicles has not been so important due to discrepant sizes caused by various measuring techniques (Chernyshev et al. 2015). More importantly, the function of EVs is mainly decided by the composition of cargo instead of the size (Lötvall et al. 2014). Even though it is known that the generation of these vesicles occurs in different sites within the cell, it seems difficult to distinguish them well

using current methods such as ultracentrifugation, sucrose gradient, polymer-based precipitation, or immunocapture, because of their overlapping range of size, similar morphology and variable composition (Clayton et al. 2001; Théry et al. 2006; Tauro et al. 2012; Tkach et al. 2018). As a result, what we isolate from body fluids *in vivo* or supernatant *in vitro* is actually a mixture containing EVs of various subtypes. According to the recommendation from ISEV (International Society for Extracellular Vesicles), "extracellular vesicle" (EV) was adopted to name the nano-sized vesicles in the present study (Théry et al. 2018), instead of exosomes which have been most often used in published articles about EVs (Gould und Raposo 2013; Lötvall et al. 2014).

Considering that there are some non-vesicular components such as lipid, protein, and RNA in the extracellular environment, it is necessary to identify the harvested EVs through several techniques such as electron microscopy or cryo-electron microscopy, nano-track analysis (NTA), and western blot analysis of surface marker proteins. Firstly, electron microscopy could show irregular-shaped membrane-enclosed morphology of single vesicles, while cryo-electron microscopy provides more accurate information about the shape and the size of the isolated vesicles (Cizmar und Yuana 2017). Secondly, NTA can be used to analyze vesicle concentration and measure the size distribution of EVs (Bachurski et al. 2019). The third method is the western blot used to recognize protein markers of EVs. In recent years, marker proteins of EVs include tetraspanins (CD9, CD63, and CD81) and proteins that are involved in the biogenesis of MVBs, such as Tumor Susceptibility Gene 101 (TSG101) and ALG2 interacting protein (Alix) (Conde-Vancells et al. 2008; Epple et al. 2012; Andreu und Yáñez-Mó 2014). Of note, we should always keep in mind that these proteins do not represent “exosome-specific” marker proteins, because different subsets of EVs may contain common markers. As previously noted, EVs contain proteins, lipids, RNAs, DNAs, and miRNAs, all of which are secreted by parent cells after the sorting and secretion process under physiological or pathological conditions. As a result, EVs would be able to reflect the biological state and characteristic function of the parent cells. Therefore, EVs are promising to become effective diagnostic methods of different diseases depending on the origin cells. At the same time, EVs have been shown to participate in cell-cell communication with both endocrine and paracrine effects since it was first described by Stahl and Johnstone in 1983 (Pan and Johnstone 1983; Regev-Rudzki et al. 2013). Based on this theory, EVs from specific cells or EVs modified *in vitro* with the loading of a particular cargo (e.g. miRNAs, siRNAs, and drugs) and then delivered to the target cells, can be a promising therapeutic method (Valadi et al. 2007; Fitzner et al. 2011; Mizrak et al. 2013) (Figure 1).

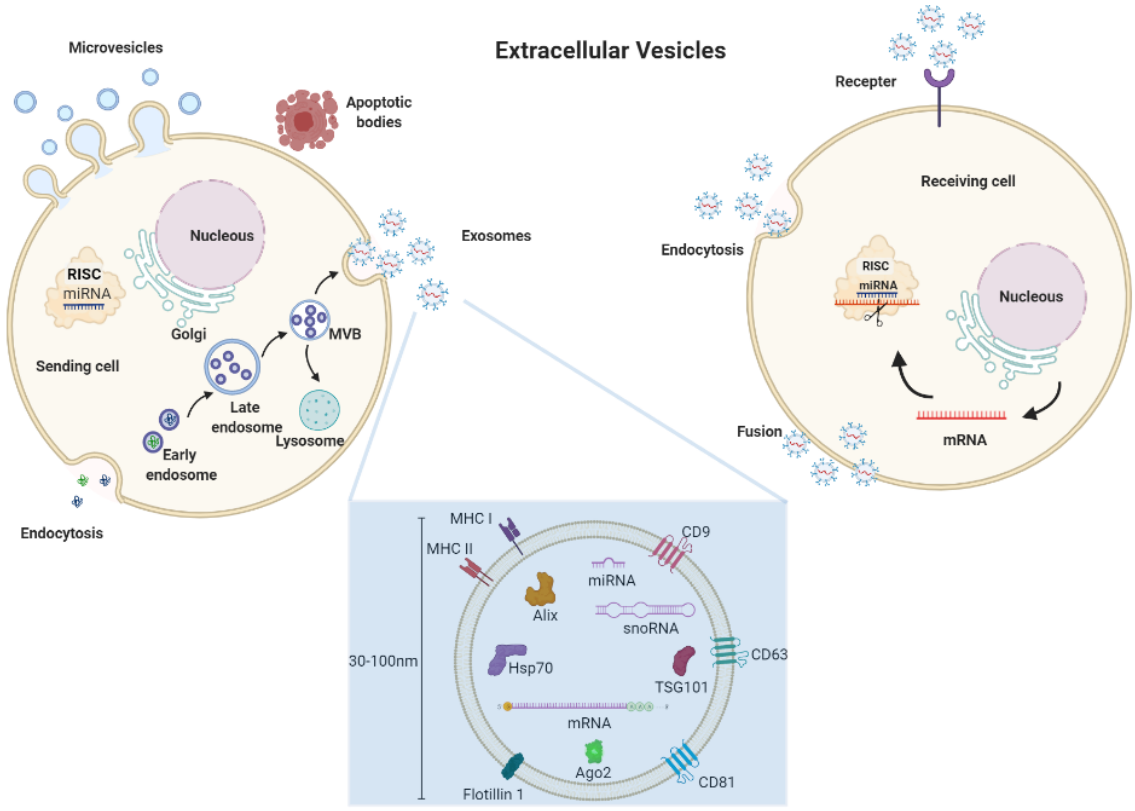

Figure 1: Illustration of cell-cell communication by EVs. EVs containing miRNAs are synthesized and secreted into extracellular space by sending cells. Thereafter, EVs can be uptaken by receiving cells. Then the cargo of EVs is released and the transferred miRNAs are loaded into the RISC complex which will further affect the gene expression of the target cell during the process of cell-cell communication.

1.7. Aim of the thesis

Despite years of research, there are still no effective treatment methods to stop or reverse the progress of OA. The main reason is that the pathogenesis of OA is still unclear due to its long-term course and complex etiology. As a result, it is impossible to cure OA with traditional medications that mainly reduce pain and swelling. Recently, studies have found miRNAs are implicated in the pathogenesis of osteoarthritis, during which *miR-221-3p* could regulate the pathophysiological process of OA by its mechanosensitive and anti-inflammatory characters in cartilage. More importantly, the latest research demonstrated that exosomal *miR-221-3p* may promote cartilage regeneration *in vivo*. Meanwhile, the subchondral bone was commonly reported to participate in the occurrence and development of OA. Considering that the presence of microchannels across the bone-cartilage interface permits cell-cell communication between these two parts, it is reasonable to speculate *miR-221-3p* may regulate the pathogenesis of OA through participation in the crosstalk between chondrocytes in cartilage and osteoblasts in the subchondral bone. Therefore, the present

study aims to research the role of EVs loaded *miR-221-3p* in the chondrocytes-osteoblasts communication *in vitro*, which could help us understand the pathogenesis of this chronic disease and even provide us with a new target to treat OA.

2. Materials and Methods

In brief, the workflow of this study is illustrated in (Figure 2).

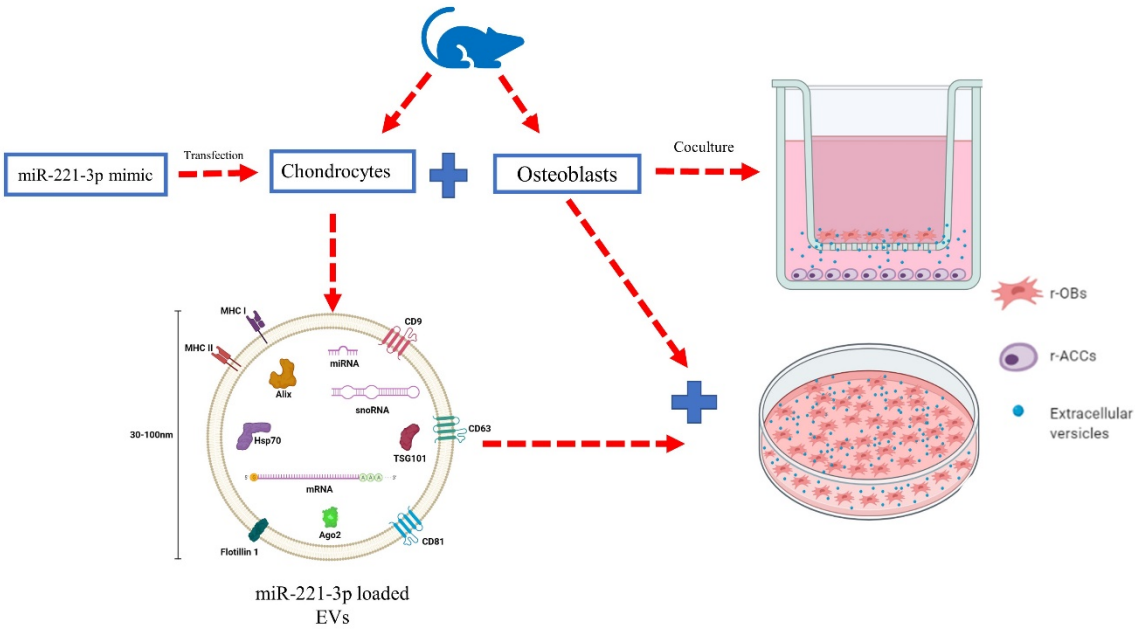

Figure 2: Illustration of workflow. Chondrocytes and osteoblasts were firstly isolated from newborn rats. *MiR-221-3p* concentration was increased by transfection methods in chondrocytes. Chondrogenic EVs were isolated, identified, and checked for *miR-221-3p* concentration. In the next step, chondrocytes were cocultured with osteoblasts to study chondrocyte-osteoblast communication. Furthermore, osteoblasts were treated by *miR-221-3p* loaded EVs derived from chondrocytes to study the effect of *miR-221-3p* loaded EVs on osteoblasts.

2.1. Isolation and culture of primary cells

Rat chondrocytes (r-ACCs) and rat osteoblast (r-OBs) were isolated according to the traditional enzyme digestion method with minor modifications (Liu et al. 2019; Muhammad et al. 2019). Briefly, 3—5 rats (born not old than 72 hours ago) were sacrificed by cervical dislocation and immediately soaked in 70% (vol/vol) alcohol for 10 minutes to clean the body surface. These sacrificed rats were transferred to the clean bench under aseptic conditions for later operations. Chondrocytes were isolated from the knee joint articular cartilage. Firstly, separate the skin of the knee joint, open the joint capsule, expose the joint cavity, isolate the cartilage (white transparent, elastic tissue) from femoral condyles and tibial plateau using scissors and tweezers and place them in pre-cooled Phosphate-Buffered Saline (PBS), rinse several times. Then transfer these tissues into Dulbecco's Modified Eagle Medium (DMEM)-low glucose containing 10% FBS and 1% penicillin/streptomycin (P/S),

remove the fascia, muscle, and connective tissue carefully, cut the cartilage into pieces less than 1mm^3. Afterwards, transfer these cartilage chips to the 15 ml falcon tube and digest them with 5 ml 0.25% trypsin for 30 minutes in a water bath at 37 °C to remove extra synovial tissue. Then centrifuge at 300 g for 5 minutes at room temperature and discard the supernatant Add 5 ml of 0.1% collagenase II dissolved in a complete medium, transfer the suspension to a 25 cm^2 flask and digest in a 37 °C, 5% CO_2 incubator for 4—6 hours. The digestion process was terminated by adding DMEM complete medium. Collect the released cells and discard the digest medium after centrifugation for 5 min at 300 g, 22°C, then resuspend the cell pellet in a new 25 cm^2 flask with DMEM complete medium and incubate these cells in a 37 ° C, 5% CO_2 incubator. Change medium every 2 days and subculture cells in 1:3 ratio when they reached 80% confluence. The osteoblasts were isolated from the calvarium using almost the same process as the chondrocytes from cartilage except for the exact position to dissect the calvarium. Then the cells mixed with 10% DMSO were stored firstly at -80°C overnight and then at -140°C until use. For the subsequent experiments, all the cells were used in passages 3—5.

2.2. Osteogenic differentiation

Rat osteoblasts were seeded in 24-well plates at a cell density of 5 x 10^4 cells/well. After 24 hours, the medium was replaced with the osteogenic differentiation medium (ODM) with or without Dexamethasone (Dexa, 100 nM). The exact components of ODM can be seen in Table 10. Change medium every 2 days. Finally, the cells were harvested at 1, 2, or 3 weeks according to specific experimental requirements.

2.3. Establishment of an OA model *in vitro*

Rat chondrocytes were seeded at 5 x 10^4 cells/well density in a 24-well plate and cultured in a DMEM-low glucose medium containing 10% FBS and 1% P/S for 24 hours. Then a medium change to an induction medium containing Interleukin 1 beta (IL-1β) (10 ng/ml) was performed and the cells were incubated for another 24 hours. This model was verified by western blot analysis to test the expression level of Cyclooxygenase2 (COX2) and qRT-PCR to test catabolic and anabolic factors such as Matrix metallopeptidase 13 (*MMP13*), a disintegrin and metalloproteinase with thrombospondin motifs 5 (*ADAMTS5*), *COX2*, and transcription factor SOX9 *(SOX9)*. All these results were compared with the control.

2.4. Transfection

Rat chondrocytes were seeded in 24-well plates at a cell density of 5 x 10^4 cells/well. After 24 hours, the medium was changed with one without FBS or antibiotics in it. Then the *miR-221-3p* mimic and scrambled control were transfected via Lipofectamine RNAiMAX according to the manufacturer's protocol. In brief, 1.5 µl Lipofectamine RNAiMAX and 50 nM *miR-221-3p* mimic or scrambled control were added per well for transfection in 24 well plates, while 7.5 µl Lipofectamine RNAiMAX and 15 µl *miR-221-3p* mimic or scrambled control were added per well for transfection in 6 well plates. After 6 hours of incubation in the incubator, the medium was changed to one containing FBS and antibiotics. Cells were incubated for 48 h and afterwards harvested for downstream experiments.

2.5. Prediction and identification of the targets of *miR-221-3p*

To predict possible targets of *miR-221-3p*, three independent platforms including miRDB (http://mirdb.org/), miRWalk (http://zmf.umm.uni-heidelberg.de/apps/zmf/mirwalk2/), Targetscan (http://www.targetscan.org/vert_72/), and were used to search for their common targets. The predicted target genes and their mRNA expression level were evaluated by qRT-PCR in the transfected cells compared with the control.

2.6. Proliferation assay

Cell proliferation was evaluated by xCELLigence RTCA DP Analyzer (ACEA Bioscience, USA) which was placed in a humidified incubator with 5% CO2, at 37 °C according to the manufacturer's instructions. In Brief, cells were seeded in a CIM plate (ACEA Bioscience, USA) at a density of 10000 cells per well and incubated in the safety cabinet for 30 minutes. The CIM plate was installed into RTCA DP Analyzer and cell proliferation was continuously monitored by RTCA Control Unit. 6 hours later, transfection of the cells with *miR-221-3p* mimic and scrambled control was performed according to 2.4. After the restoration of the CIM plate into the RTCA DP Analyzer, the impedance value of each well was automatically recorded every 30 minutes by the xCELLigence system for a duration of 96 hours and shown as a cell index (CI) value which was further analyzed by RTCA Data Analysis Software 1.0 (ACEA Bioscience, USA).

2.7. Coculture of r-ACCs and r-OBs

Rat osteoblasts were seeded in 6-transwell inserts (upper chamber) (Merck KGaA, Darmstadt, Germany) at a density of 5 x 10^4 cells/well, and the r-ACCs were seeded in the 6-well plates (lower chamber) at a density of 3 x 10^5cells/well. The cells were cultured for 24 hours in DMEM-low glucose containing 10% FBS and 1% P/S. Then the transfection of r-ACCs with *mir-221-3p* mimic or scrambled control was performed for 6 hours in a medium without FBS or antibiotics. Washing of r-ACCs and r-OBs with PBS 2 times and coculturing them with DMEM-low glucose containing 10% FBS free of EVs and 1% P/S in transwell plate for 48 hours (2.6 ml medium for r-ACCs and 1.5 ml for r-OBs). R-ACCs, r-OBs, and the supernatant were collected for further analysis respectively.

2.8. Isolation of EVs

Cell culture supernatant was harvested after 72 hours' incubation with cells and successively centrifuged at 500 x g for 5 minutes and 2000 x g for 30 minutes. The supernatant was filtered through a 220 nm filter and mixed (1:5) with Polyethylene glycol (PEG) (Sigma-Aldrich, USA) solution (500 mg/ml in PBS), which was then incubated overnight at 4 °C and centrifuged at 1500 x g for 30 minutes. The resulting pellets were dissolved in 100 µl PBS and stored at 4 °C until further use. All centrifugation steps were performed at 4 °C.

2.9. Nanoparticle Tracking Analysis

Nanosight platform (NanoSight LM10, Malvern Panalytical, Kassel, Germany) was used to measure the size distribution and particle concentration of EVs. In brief, the EV sample was firstly diluted 1000 times with PBS. After the diluted sample (around 0.5 ml) was added to the device, the screen gain was set as 1.0, the camera level was set to 14 and the capture time was 60 seconds. During the detection process, the screen gain was set as 10.0 and the detection threshold was set as 4. Each sample was repeated 3 times and the averaged result of the size distribution of EVs was further calculated by NTA software 2.3 and illustrated by Graphpad Prism 5 (GraphPad Software, USA).

2.10. Treat r-OBs EVs

Rat Osteoblasts were seeded in 24-well plates at a density of 5 x 10^4 cells/well. After 24 hours a certain amount of EVs were added into the medium. 48 hours later, cells were harvested for further analysis.

2.11. RNA isolation and quantitative real-time PCR analysis

Total RNA was extracted using Trizol reagent (Invitrogen, USA) according to the manufacturer's instructions. Briefly, remove the medium from the well and add 500 µl Trizol reagent followed by pipetting up and down to fasten lysis, then the samples were stored at -20°C or for the next step. After 5 minutes' incubation at room temperature (RT), add 100 µl chloroform per tube and incubate 3 minutes at RT. Then centrifuge 15 minutes at 12000 x g at 4° C, and transfer the aqueous phase to another new tube without contamination of the other two phases. Afterwards, add 250 µl 100% isopropanol per tube and incubate 10 minutes at RT. Thereafter, centrifuge 10 minutes at 12000 x g at 4° C, and remove isopropanol by pipetting carefully in case the RNA pellets are lost. Wash the pellet with 500 µl 70% ethanol per tube and centrifuge 10 minutes at 76000 x g at 4° C. Then remove the ethanol by pipetting and centrifuge again shortly for collecting drops. Remove the rest ethanol and dry for 5-10 minutes until the pellet turns gelly. In the end, resuspend the pellet in 20 µl RNase-free water. RNA concentration and quality were measured with a DS-11 FX/FX+ integrated spectrophotometer (Thermo Fisher Scientific, USA). Thereafter, the RNA samples were stored at -80 degrees until further use. For the quantitative real-time PCR analysis of mRNA, 1000 ng of total RNA was reverse transcribed into complementary DNA (cDNA) in a total volume of 20 µl by adding the components described in Table 1. The qRT-PCR reaction was performed according to the standard protocol (Table 3) in a total volume of 20 µl by adding the components described in Table 2. *GAPDH* was used as a housekeeping gene to normalize the results and the information of primers was listed in Table 7. For the quantitative real-time PCR analysis of miRNA, 10ng of total RNA was reverse transcribed in a total volume of 10µl with miRCURY LNA RT Kit (QIAGEN, Germany) according to the manufacturer's protocol (Table 4). The qRT-PCR reaction was performed according to the standard protocol (Table 6) by using miRCURY LNA SYBR Green PCR Kit (QIAGEN, Germany) with the miRNA-specific forward primer and the universal reverse primer (QIAGEN, Germany) as described in Table 5. U6 small nuclear

RNA was used to normalize the results. All the calculations for the relative results adopted the standard $2^{-\Delta\Delta Ct}$ method and were illustrated by Graphpad Prism 5.

Table 1: Pipetting scheme for reverse-transcribed mRNA

Component	Volume
mRNA and Distilled water	15 µl
iScript Reverse Transcriptase	1 µl
r5x iScript Reaction buffer	4 µl

Table 2: Pipetting scheme for mRNA qRT-PCR reaction

Component	Volume
cDNA	1 µl
Forward Primer (10 µM)	1 µl
Reverse Primer (10 µM)	1 µl
SYBR buffer	10 µl
Distilled water	8 µl

Table 3: Standard protocol for mRNA qRT-PCR reaction

Step	Description	Time and Temperature
1	Initial denaturation	3 min, 95 °C
2	Denaturation	10 sec, 95 °C
3	Annealing	10 sec, 55 °C
4	Final amplification	30 sec, 72 °C
5	Number of cycles	40

Table 4: Pipetting scheme for reverse-transcribed miRNA

Component	Volume
mRNA (5 ng/µl)	2 µl
10 x miRCURY RT Enzyme Mix	1 µl
5 x miRCURY RT Green Reaction Mix	2 µl
Distilled water	4.5 µl

Table 5: Pipetting scheme for miRNA qRT-PCR reaction

Component	Volume
cDNA (60 x dilution)	3 µl
Forward Primer	1 µl
Reverse Primer	1 µl
buffer	5 µl
Distilled water	2 µl

Table 6: Standard protocol for miRNA qRT-PCR reaction

Step	Description	Time and Temperature
1	Initial denaturation	2 min, 95 °C
2	Denaturation	10 sec, 95 °C
3	Combined annealing /extension	60 sec, 56 °C
4	Number of cycles	40

Table 7: Sequence information of qRT-PCR primers

Internal number	Gene name	Primer sequence
201	rGAPDH F	CTC ATG ACC ACA GTC CAT GC
202	rGAPDH R	TTC AGC TCT GGG ATG ACC TT
203	rADAMTS5 F	TGT GGT GCG CCA AGG CCA AA
204	rADAMTS5 R	CCC TGT GCA GTA GCG GCC AC
205	rMMP13 F	AAG ATG TGG AGT GCC TGA TG
206	rMMP13 R	CCA GTG TAG GTA TAG ATG GGA AC
207	rADAMTS4 F	ACA ATG GCT ATG GAC ACT GCC TCT
208	rADAMTS4 R	TGT GGA CAA TGG CTT GAG TCA GGA
209	rCOX2 F	GTG GGA TGA CGA GCG ACT G
210	rCOX2 R	CCG TGT TCA AGG AGG ATG G
249	rCDKN1B F	TCAAACGTGAGAGTGTCTAACG
250	rCDKN1B R	CCGGGCCGAAGAGATTTCTG
251	rMMP2 F	CAAGTTCCCCGGCGATGTC
252	rMMP2 R	TTCTGGTCAAGGTCACCTGTC
253	rTIMP3 F	CTTCTGCAACTCCGACATCGT
254	rTIMP3 R	GGGGCATCTTACTGAAGCCTC
255	rARNT F	GACAGACCACAGGACAGTTCC
256	rARNT R	AGCATGGACAGCATTTCTTGAA
257	rTCF7L2	CGCTGACAGTCAACGCATCTATG
258	rTCF7L2	GAGGACTCCTGCTTGACTGTC
262	rCOL2A1 F	GCCAGGATGCCCGAAAATTAG

Table 7: Sequence information of qRT-PCR primers (continued)

263	rCOL2A1 R	GGCTCCGGGAATACCATCAG
264	rSOX9 F	TCCCCGCAACAGATCTCCTA
265	rSOX9 R	AGCTGTGTGTAGACGGGTTG
266	rTIMP2 F	TGGGAACGTGCATTTTGCAG
267	rTIMP2 R	AAACACTGGTTGGAGGGCAA
268	rDKK2 F	ATTGTGCACCTCGTCTGTGT
269	rDKK2 R	TCCCCTCATGGGTCAGACAT
270	rAXIN2 F	TGCAATGGGTTCAGGCAGAT
271	rAXIN2 R	CCCGGAGAGTTTTGCTGGAT
272	rMAPK10 F	AGGTGTGTGTTCCTTACAGGT
273	rMAPK10 R	CATCATGAAGCTTGTGCCCG
60	rCOL1A1 F	GTGCGATGACGTGATCTGTGA
61	rCOL1A1 R	CGGTGGTTTCTTGGTCGGT

2.12. Immunofluorescence

Rat chondrocytes were seeded on coverslips in 24-well plates at a density of 5 x 10^4 cells/well. After 24 hours, the cells were washed 3 times with PBS. Thereafter, the cells were fixed with 4 % formaldehyde for 10 minutes and washed 3 times with PBS. Afterwards, a permeabilization step was performed with 0.2 % Triton-100 for 10 minutes and three subsequent washes with PBS. For blocking 5 % skim milk was used and incubated for 30 minutes at room temperature and followed by 3 washes with PBS. The primary collagen II antibody (Rabbit, Abcam, ab34712, 1:50) was diluted in PBS and incubated overnight at 4 °C. Three thorough washes with PBS were done to remove the unbound primary antibody. This was followed by 2 hours of incubation with the secondary antibody (Anti-rabbit, Invitrogen, R37117, 1:500). The secondary antibody was aspirated and followed by 3 washes with PBS. A drop of DAPI (Sigma-Aldrich, USA) was applied on a microscope slide and the

coverslip with cells upside down was transferred on this drop. The preparation was ready for microscopy after polymerization at 4°C overnight.

2.13. Von Kossa staining

Rat osteoblasts were differentiated as described above (2.2). After 2 weeks, the samples were rinsed 3 times with PBS and fixed with 4 % formaldehyde for 10 minutes. Then the samples were washed in several changes of distilled water. The samples were incubated with 1% silver nitrate solution under ultraviolet light for 1 minute. The un-reacted silver was removed with 5% sodium thiosulfate for 5 minutes and rinsed again in distilled water. The preparation was ready for visual study and microscopy.

2.14. Alizarin red staining

Rat osteoblasts were differentiated as described above (2.2). After 2 weeks, they were washed 3 times with PBS and fixed with 4 % formaldehyde for 10 minutes and rinsed 3 times with distilled water. The staining of the samples was performed with the Alizarin Red Solution for 10 minutes. Rinsed in distilled water. The preparation was ready for visual study and microscopy.

2.15. Preparation of EVs or cellular samples for protein analysis

Rat chondrocytes were seeded in 6-well plates at a density of 3 x 10^5 cells/well. After a period of culture, the cells were washed 3 times with PBS, and 100 µl RIPA buffer was added and incubated for 30 minutes at 4 °C. After Pipetting up and down, cell lysates were transferred to a 1.5 ml tube. Then centrifuged at 16000 x g for 20 minutes at 4°C. Afterwards, the supernatant was collected in fresh tubes and placed on ice. The 4 x Laemmli loading buffer (Bio-Rad, USA) was added to the protein samples according to the 1:4 ratio and the mixture was then boiled at 95 °C for 5 minutes. Finally, these samples were stored at -20 °C until use. The protocol to isolate proteins from EVs was almost the same as described above with one exception. The pellet of EVs at the end of the isolation procedure was dissolved in 100µl RIPA buffer instead of PBS. Then BCA Protein Assay Kit (Thermo Fisher, USA) was used to treat protein samples according to the manufacturer's protocol. Afterwards protein concentration was measured by a DS-11 FX/FX+ integrated spectrophotometer (Thermo Fisher Scientific, USA). A standard curve (0 ng/µl, 100 ng/µl, 200 ng/µl, 500 ng/µl, 1000 ng/µl, and 2000 ng/µl) was used to calculate protein concentration.

2.16. Polyacrylamide gel electrophoresis

SDS-polyacrylamide gel electrophoresis (SDS-PAGE) was adopted to separate proteins based on their molecular weight. 12% gels were prefabricated with the kit in cassettes (Bio-Rad, USA) according to the manufacturer's protocol. Afterwards, the polymerized gel was inserted into the electrophoresis chamber (Bio-Rad, USA) which was filled with electrophoresis buffer (Bio-Rad, USA). Protein samples were added into the channel of the gel (10 µg total protein/channel), while 3 µl Pageruler Prestained Protein Ladder (Bio-Rad, USA) was used to quantify the molecular weight of proteins. The whole process of electrophoresis was completed at 200 V for 30 mins.

2.17. Western Blot

After the electrophoresis, proteins were further transferred to a PVDF membrane (Bio-Rad, USA). The whole transfer process was performed inside Trans-Blot Turbo Transfer System (Bio-Rad, USA) according to the manufacturer's protocol. After 7 minutes transfer at 25 V, the membrane was blocked with 5 % skim milk dissolved in deionized water for 1 hour at RT. Afterwards, the membrane was incubated with a primary antibody (1:1000 in 5 % skim milk dissolved in deionized water) overnight at 4 °C. The next day the membrane was washed with TBS-T solution 3 x 5 minutes, then incubated with HRP coupled secondary antibody (1:10.000 in TBS-T solution) for 1 hour at room temperature. Thereafter, the membrane was washed with TBS-T 3 x 5 minutes. Subsequently, the rinsed membranes were soaked in ECL chemiluminescence reagent (Bio-Rad, USA) and the blots were exposed with the imaging system ChemiDoc XRS+ (Bio-Rad, USA). The results were further analyzed via Image Lab Software (Bio-Rad, USA). The antibodies used are listed in Table 8.

Table 8: Antibody information

Antibody	Concentration	Supplier	Cat. No.	Species
Anti-β-actin	1:1.000	Sigma Aldrich	A2066	mouse
Anti-COX2	1:1.000	Abcam, UK	ab15191	rabbit
Anti-COL2	1:50	Abcam, UK	ab34712	rabbit
Anti-Alix	1:1.000	Santa Cruz, USA	sc-53538	mouse

Table 8: Antibody information (continued)

Anti-TSG101	1:1.000	Santa Cruz, USA	sc-7964	mouse
Anti-CD81	1:1.000	Santa Cruz, USA	sc-166029	mouse
Anti-rabbit	1:10.000	Invitrogen, USA	G-21234	goat
Anti-mouse	1:10.000	Invitrogen, USA	G-21040	goat

2.18. Schematic diagram

All the schematic diagrams in this thesis were created with BioRender.com (BioRender, Canada) and Microsoft Office PowerPoint 2016 (Microsoft, USA).

2.19. Statistical analysis

The data of the whole experiment were statistically analyzed by GraphPad Prism 5. The Mann-Whitney-U-Test was adopted to compare two groups while the one-way ANOVA followed by Tukey's post-hoc-test was specifically selected for the comparison of more than two groups. Unless otherwise stated, results were shown as mean values with SD, and there were statistical differences when the *P*-value was less than 0.05.

2.20. Machines

Table 9: Used machines and manufacturer information

Machine	Model	Company
Balance	Explorer	Ohaus, USA
Centrifuge	Heraeus Multifuge X1R	Thermo Fisher, USA
Centrifuge	Microcentrifuge 5415	Sigma-Aldrich, Germany
Centrifuge	Heraeus Multifuge X1R	Thermo Fisher, USA
Freezer (-80 °C)	DF9014	IlShin, Netherlands
Freezer (-150 °C)	ULT10140-9-M23	Thermo Fisher, USA

Table 9: Used machines and manufacturer information (continued)

Pipette	Eppendorf Pipette	Thermo Fisher, USA
Ice machine	ZBE 70-35	Ice Systems, UK
Incubator	Cytoperm 2	Thermo Fisher, USA
Incubator	BBD 6220	Thermo Fisher, USA
Microscope	DMi8	Leica, Germany
Safety Cabinet	Heraeus HS12	Thermo Fisher, USA
Water bath	Isotemp GPD 20	Thermo Fisher, USA
Vortexer	RS-VA10	Phoenix Instrument, Germany
Real-time cell analyzer	xCELLigence® RTCA DP	ACEA Bioscience, USA
Western Blot chamber	Mini Tetra Cell	Bio-Rad, USA
Western Blot transfer system	Trans-Blot Turbo Transfer System	Bio-Rad, USA
Western Blot transfer system	Criterion Blotter	Bio-Rad, USA
ECL machine	Chemocam Imager	INTAS, Germany
Spectrometer	DS-11 FX +	Thermo Fisher, USA
Real-Time PCR	CFX96 system	Bio-Rad, USA
Real-Time PCR	CFX384 system	Bio-Rad, USA
Printer	FS-C5150DN	Kyocera, Germany
Shaker	PMS-1000i	Avantor, US
Shaker	B3D2300	Benchmark, US
Thermo-Shaker	PCMT-H18	Grant-bio, UK
Revers transcription	Labcycler 012-103	SensoQuest

2.21. Buffers and Solutions

Table 10: Information about buffers and solutions

Buffer and solutions	Recipe
RIPA buffer	25 mM Tris-HCl pH 7,6 150 mM NaCl 1 % NP-40 1 % Sodium deoxycholate 0,1 % SDS
Western blot transfer buffer(1x)	Tris: 4.5 g Glycine: 21.6 g Methanol: 300 ml Water: 1200 ml
Osteogenic differentiation medium (ODM)	DMEM-Low glucose 10 % FCS 1 % penicillin-streptomycin 0.2 mM ascorbic acid-2-phosphate 10 mM β-glycerophosphate

2.22. Chemicals and Materials

Table 11: Chemicals

Compounds	Provider Information
Dimethyl sulfoxide	Sigma-Aldrich, USA
DAPI	Sigma-Aldrich, USA
Dexamethasone	PAN, Germany
Trypsin	Pan Biotech, Germany
Ethanol	Carl Roth, Germany
Formaldehydlsg. 4 %	Fischer/chemsolute, Germany

Table 11: Chemicals (continued)

Methanol	Merck, USA
β-Glycerophosphate disodium salt pentahydrate	Roth, Germany
L-Ascorbic Acid 2-phosphate	Cayman chemical company
Glycine	AppliChem, Germany
TRIS	Roth, Germany
Polyethylene glycol	Sigma-Aldrich, USA
Sodiuiumthiosulfat-5-hydrate	Merck, USA
Silver nitrate	Paesel & Lorei, Germany
Alizarin Red S staining solution	Morphisto, Germany
Triton X-100	AppliChem, Germany
Powdered milk	Roth, Germany
10 x Tris/Glycine/SDS Buffer	Bio-Rad, USA
TGX stain-Free FastCast Acrylamide Kit, 12 %	Bio-Rad, USA
Trans-Blot Turbo 5x Transfer Buffer	Bio-Rad, USA
Mini-PROTEAN TGX Gels	Bio-Rad, USA
Western ECL Substrate	Bio-Rad, USA
Mini-size LF PVDF Membrane	Bio-Rad, USA
Mini-size Transfer Stacks	Bio-Rad, USA
BCA Protein Assay Kit	Thermo Fisher, USA
Laminine	Bio-Rad, USA
TBS-Tween tablets	Medicago, USA
Mini-PROTEAN Glass plates	Bio-Rad, USA
Mini-PROTEAN Short plates	Bio-Rad, USA

Table 11: Chemicals (continued)

Mini-PROTEAN Gel releasers	Bio-Rad, USA
Mini-PROTEAN system casting stand	Bio-Rad, USA
Ammonium persulfate analytical grade	Bio-Rad, USA
HRP substrate	Bio-Rad, USA
SYBR Green Supermix	Bio-Rad, USA
iScript Reverse Transcriptase	Bio-Rad, USA
5 x iScript Reaction buffer	Bio-Rad, USA
miRNA PCR Kit	QIAGEN, Germany
Typan Blue Stain 0.4 %	Gibco, USA
miR-221-3p mimic	QIAGEN, Germany
miRNA scramble	QIAGEN, Germany
Lipofectamine RNAiMAX	Thermo Fisher, USA
Trizol Reagent	Ambion, USA
chloroform	Merck, USA
isopropanol	Geyer, Germany

Table 12: Materials

Consumables	Provider Information
96-well plate	Thermo Fisher, USA
24-well plate	Greiner bio-one, Germany
6-well plate	Greiner bio-one, Germany
6-transwell	Merck KGaA, Germany
CIM plate	ACEA Bioscience, USA
Serological pipette 5 ml	Sarstedt, Germany

Table 12: Materials (continued)

Serological pipette 10 ml	Sarstedt, Germany
Serological pipette 25 ml	Sarstedt, Germany
Microtube 1.5 ml SafeSeal	Sarstedt, Germany
Pipette tips 10 µl	Biozym, USA
Pipette tips 100 µl	Biozym, USA
Pipette tips 1000 µl	Biozym, USA
Pipette Reference 10 ml	Eppendorf, Germany
Pipette Reference 100 ml	Eppendorf, Germany
Pipette Reference 1000 ml	Eppendorf, Germany
Culture flask T25	Sarstedt, Germany
Culture flask T75	Sarstedt, Germany
Culture flask T175	Sarstedt, Germany
Mr. Frosty Freezing Container	Thermo Fisher, USA
Syringe 10 ml	BD, USA
Falcon tube 15 ml	Sarstedt, Germany
Falcon tube 50 ml	Sarstedt, Germany
CryoPure Tube 1.0 ml	Sarstedt, Germany
Cell Scraper	CytoOne, USA
Gloves	TH.GEYER, Germany
96 well plate for PCR	Biozym, USA
384 well plate for PCR	Thermo Fisher, USA
0.2 ml tube for PCR	Biozym, USA
Microseal 'B' seal Seals for PCR	BIO-RAD, Germany

2.23. Cell culture media and additives

Table 13: Different mediums for cell culture use.

Medium	Additives	Company
DMEM	+ L-Glutamine, + phenol red, low glucose	Gibco
OptiMEM	+ L-Glutamine, + phenol red	Gibco
DPBS	No Ca, no Mg, no phenol red	PAN
Fetal calf serum	Heat inactivated	Gibco
Trypsin	0,05 % in PBS, no Mg2+, no Ca2+	PAN
Antibiotic	penicillin-streptomycin	PAN

2.24. Software

Table 14: Different Softwares for data analysis

Software	Manufacturer
Leica Application Suite X 3.4.2.18368	Leica, Germany
Microsoft PowerPoint 2016	Microsoft, USA
Microsoft Word 2016	Microsoft, USA
Microsoft Excel 2016	Microsoft, USA
GraphPad Prism 5 (University of Göttingen licence)	GraphPad Software, USA
RTCA Data Analysis Software 1.0	ACEA Bioscience, USA
Image lab	Bio-Rad, USA
Image J	LOCI, USA
BioRender.com	BioRender, Canada

3. Results

3.1. Identification of chondrocytes and osteoblast

To identify r-ACCs, cell morphology was observed under a microscope, and immunofluorescence (IF) technology was used to test the expression of collagen II (COL2).

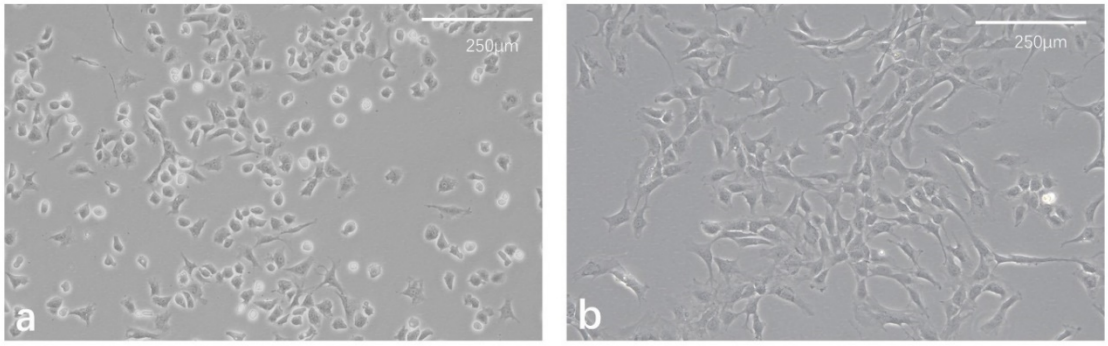

Figure 3: Morphology of chondrocytes and osteoblasts. a. Typical chondrocytes from the articular cartilage of newborn rats looked like "cobble stones". b. Osteoblasts from the calvarium of newborn rats showed irregular shapes such as triangles, fusiform, and polygon.

As shown in Figure 3a, the cells exhibited a typical "Cobblestone" morphology (Goldring 2005). IF demonstrated that the majority of r-ACCs expressed chondrocyte-specific marker COL2 (Figure 4).

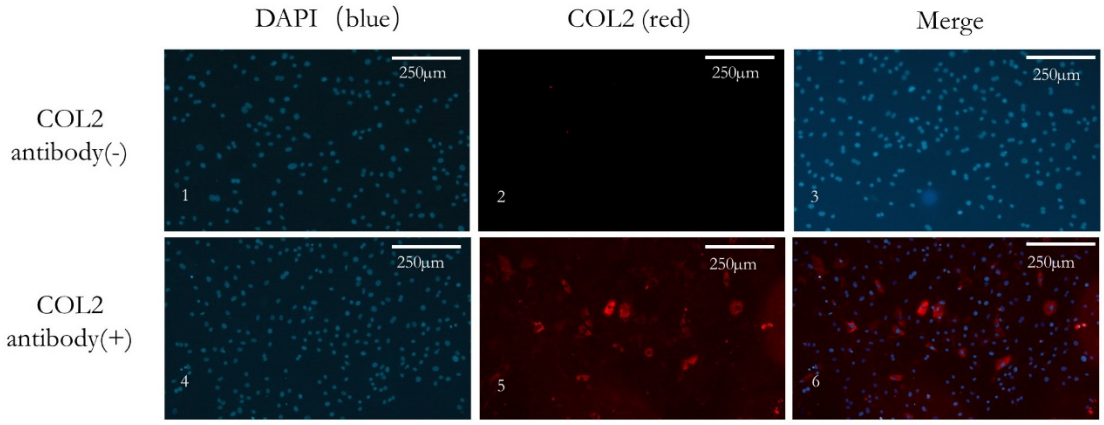

Figure 4: Identification of chondrocytes. Microscopic images showing chondrocytes positive for COL2 antibody (+) compared with negative control (-). DAPI was used as a counterstain for the cell nuclei.

It is known that r-OBs are characterized by osteogenic capacity. Rat osteoblasts, isolated from rat calvarium, were cultivated in an osteogenic differentiation medium for 1, 2, and 3 weeks. After 2 and 3 weeks of osteogenic differentiation, the cells showed positive mineralized nodule formation analyzed by von Kossa staining and Alizarin red staining, although there was no obvious difference of calcium deposits between these two-time points (Figure 5 and Figure 6). Therefore, 2 weeks' time point was selected as the osteogenic differentiation time for later experiments.

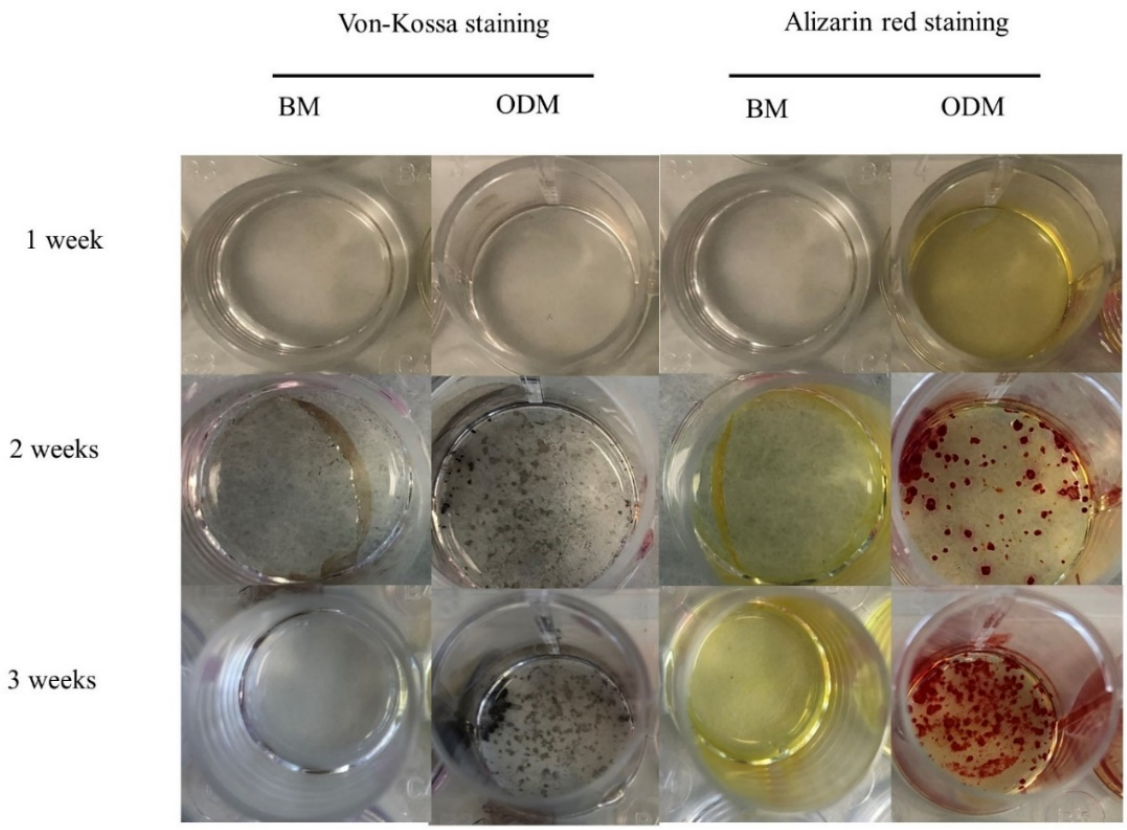

Figure 5: Macroscopic images of the Von Kossa and Alizarin red staining after 1 week, 2 weeks, and 3 weeks' osteoblasts culturing in ODM and BM. They didn't show positive staining after 1 week in culture, while both Von Kossa staining and Alizarin red staining results were positive after 2 and 3 weeks in culture in ODM compared to BM. Basal medium (BM), Osteogenic differentiation medium (ODM).

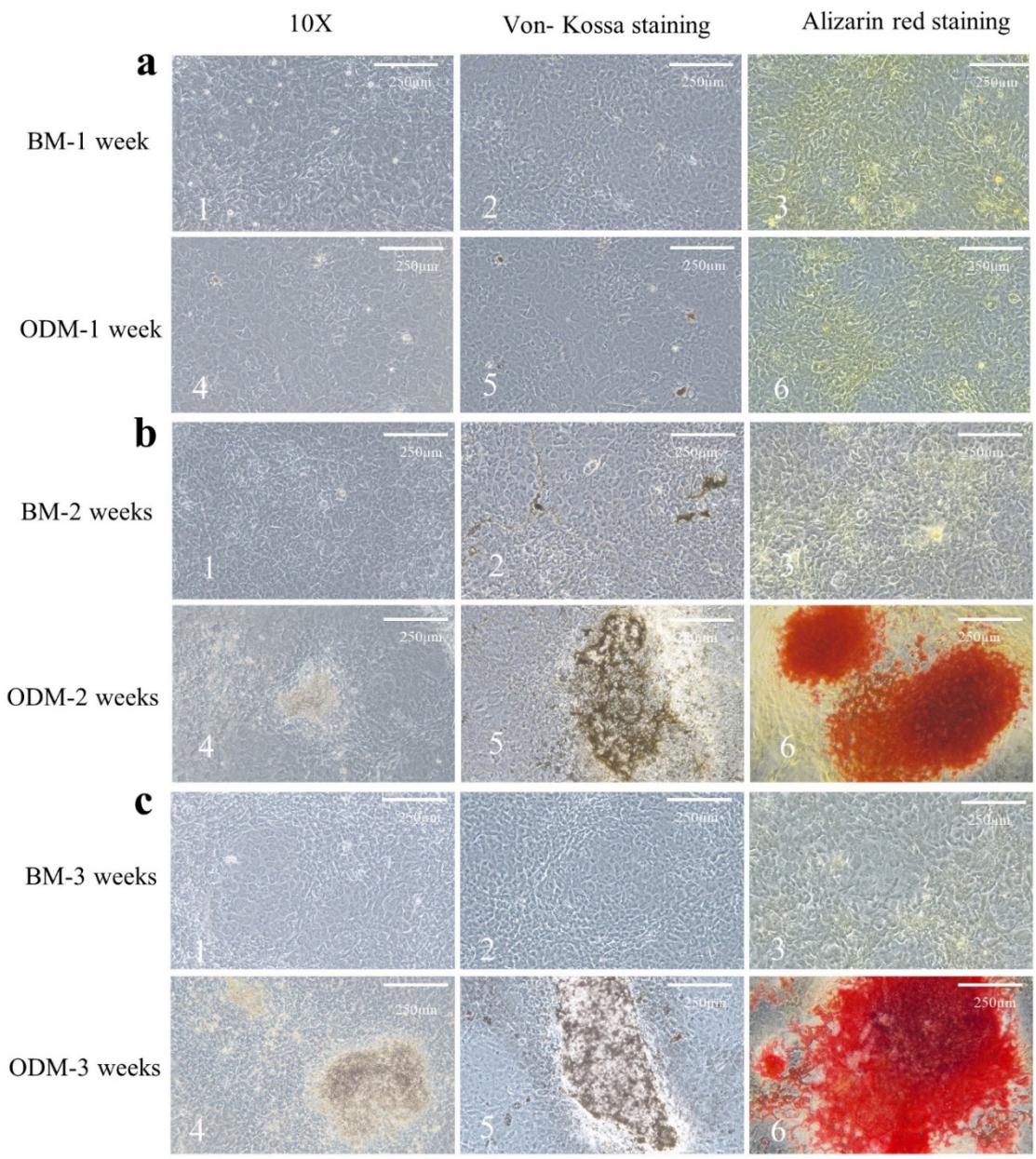

Figure 6: Microscopic images showing staining results after 1, 2, and 3 weeks' culture in ODM and BM. The osteoblasts didn't show positive staining results after one week's culture, while both Von Kossa staining and Alizarin red staining results were positive after 2 and 3 weeks' culture in ODM compared to BM.

As expected, the mRNA expression level of osteogenic markers like Collagen Type I Alpha 1 Chain (*COL1A1)*, Runt-related transcription factor 2 (*RUNX2)*, and Osteocalcin (*OCN)* were all increased after 2 weeks' osteogenic differentiation (Figure 7).

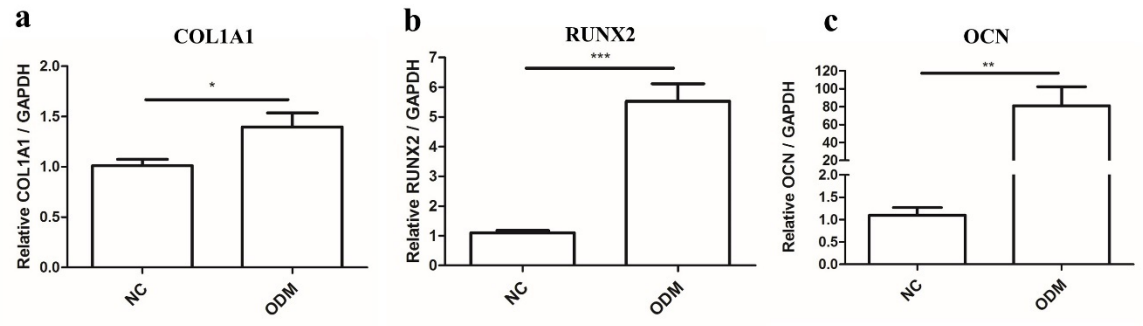

Figure 7: Relative gene expression in osteoblasts after 2 weeks' osteogenic differentiation in ODM and BM. The expression level of *COL1A1*, *RUNX2*, and *OCN* were significantly upregulated in osteoblasts treated with ODM for 2 weeks vs. corresponding control. *COL1A1*, *RUNX2*, and *OCN* relative to *GAPDH*. **P*<0.05, ***P*<0.01 and ****P*<0.001 vs. corresponding control.

Furthermore, the osteogenic differentiation capacity of the osteogenic differentiation medium (ODM) with or without dexamethasone (Dexa) on the 2 weeks' osteogenic differentiation of r-OBs were compared. Dexa treatment was able to decrease the bone formation capacity of r-OBs (Figure 8 and Figure 9).

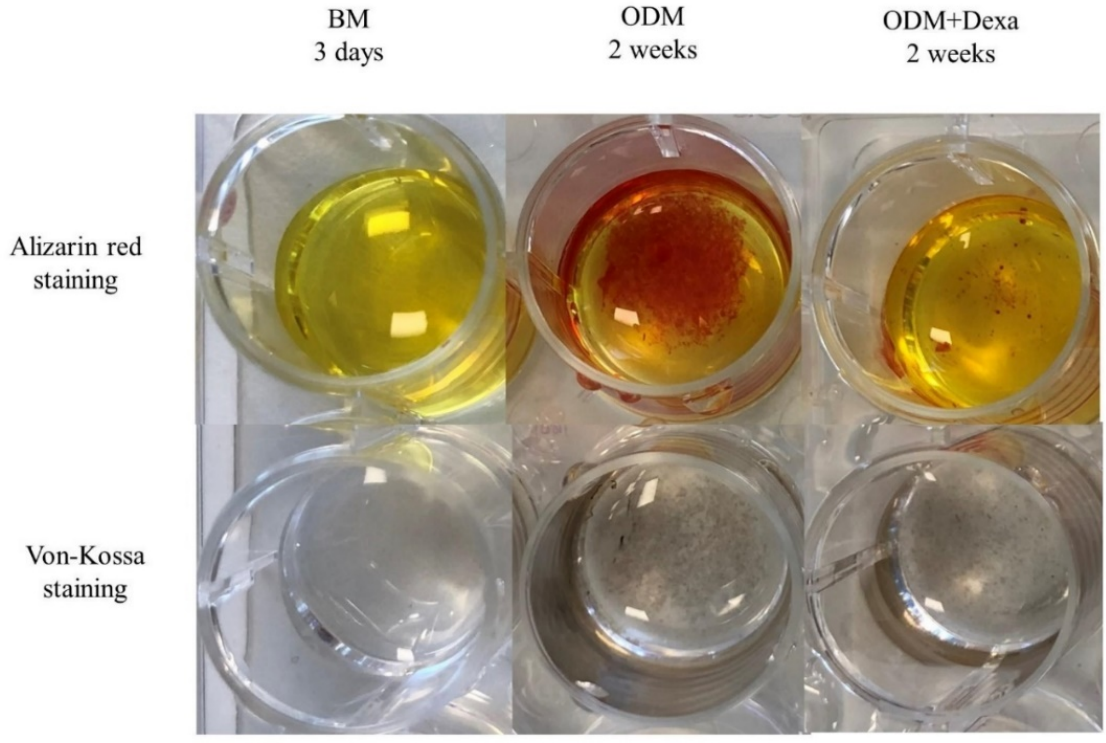

Figure 8: Macroscopic images showing positive staining results after 2 weeks' osteogenic differentiation in ODM with or without Dexa compared with the control. The results demonstrated that Dexa inhibited the bone formation capacity of osteoblast significantly.

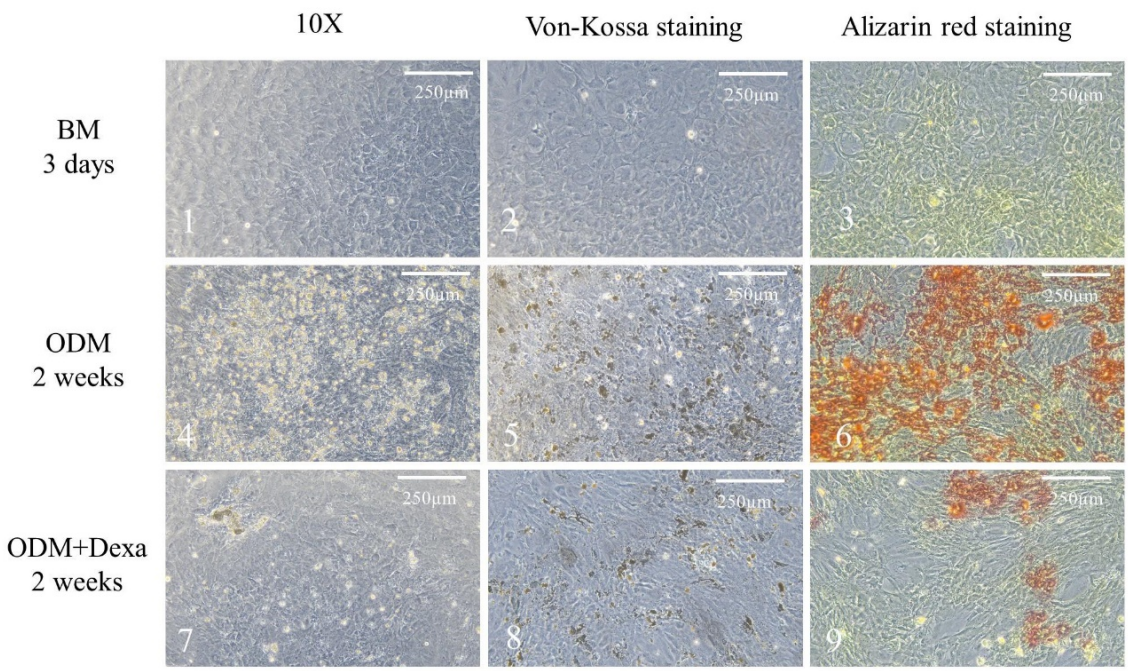

Figure 9: Microscopic images showing staining results after 2 weeks' osteogenic differentiation in ODM with or without Dexa compared with control. The results demonstrated that Dexa inhibited the bone formation capacity of osteoblast significantly.

Meanwhile, the expression level of osteogenic markers *COL1A1*, *RUNX2*, and *OCN* supported the staining results and showed a significant decrease in the Dexa-treated group compared with the control group (Figure 10). The cell morphology was observed under the microscope and r-OBs showed irregular shapes such as triangle, fusiform, and polygon (Figure 3b).

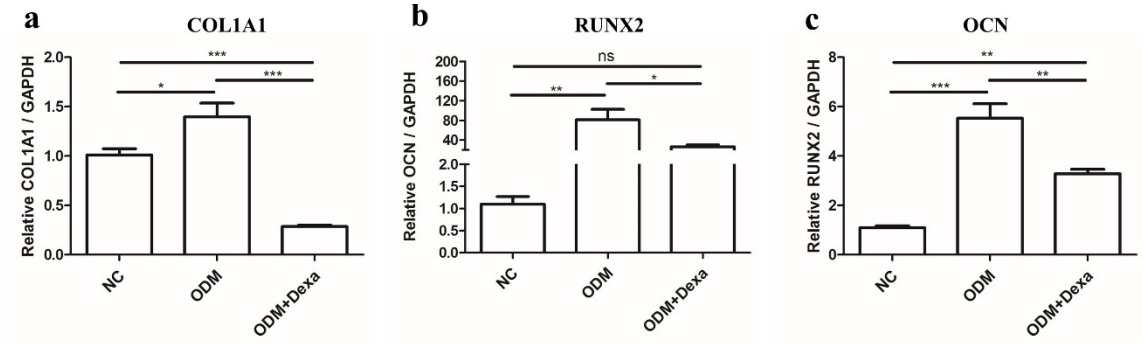

Figure 10: Relative gene expression in osteoblasts after 2 weeks' osteogenic differentiation in ODM with or without Dexa compared with control. The expression level of *COL1A1*, *RUNX2*, and *OCN* were significantly downregulated in osteoblasts treated with ODM containing Dexa for 2 weeks vs. ODM. *COL1A1*, *RUNX2*, and *OCN* relative to *GAPDH*. ns stands for not statistically significant, **P*<0.05, ** *P*<0.01, and ****P*<0.001 vs. corresponding control.

3.2. Identification of extracellular vesicles

EVs were isolated from a conditioned medium of chondrocytes with the PEG precipitation method. Nanoparticle tracking analysis (NTA) demonstrated that the size distribution of most EVs ranged from 100 to 200 nm. Characteristic marker CD81 was positively expressed in EVs based on Western blot analysis (Figure 11).

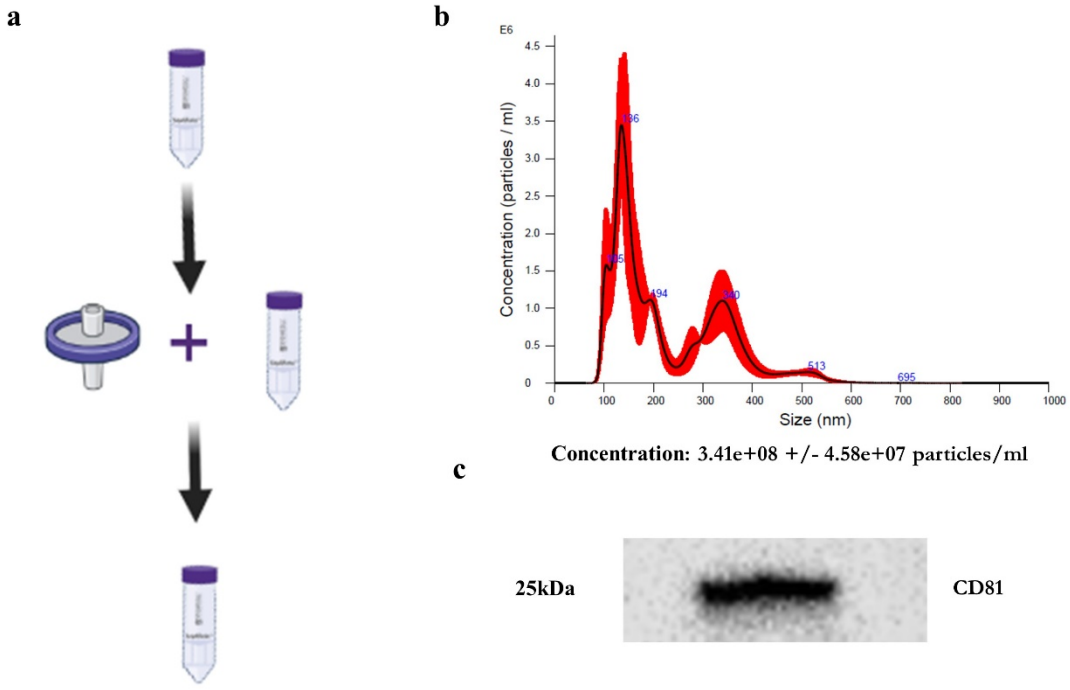

Figure 11: Isolation and identification of EVs. a. Illustration of workflow to isolate EVs by PEG precipitation method. In brief, firstly collect supernatant, centrifuge at 4 °C, 500 g for 5 min and 2000 g for 20 min to remove cells and cell debris respectively. Secondly, a 220 nm filter was used to remove microvesicles and then mix filtered supernatant with PEG solution(500 mg/ml) for 16 hours at 4 °C. Finally, centrifuge at 4 °C, 1500 g for 30 min and dissolve resulting pellet with 100 µl PBS. b. The particle size distribution of extracellular vesicles isolated by the PEG precipitation method was determined by NTA. c. EVs-specific CD81 protein measured using western blotting.

3.3. Establishment of an OA model *in vitro*

To be able to model OA *in vitro,* r-ACCs were treated with IL-1β for 24 hours. Which was evaluated with the relative expression of catabolic and anabolic genes in the treated cells compared to the control (Figure 12a-d). The expression of catabolic genes *MMP13*, *ADAMTS5*, and *COX2* was shown to be upregulated in IL-1β treated r-ACCs, by qRT-PCR, while the anabolic gene *SOX9* was downregulated in the IL-1β treated cells. Western blot analyses further confirmed that COX2 was overexpressed in the IL-1β treated group (Figure

13). Furthermore, stimulation with IL-1β resulted in a significant decrease in the expression of *miR-221-3p* compared with negative control (Figure 12e).

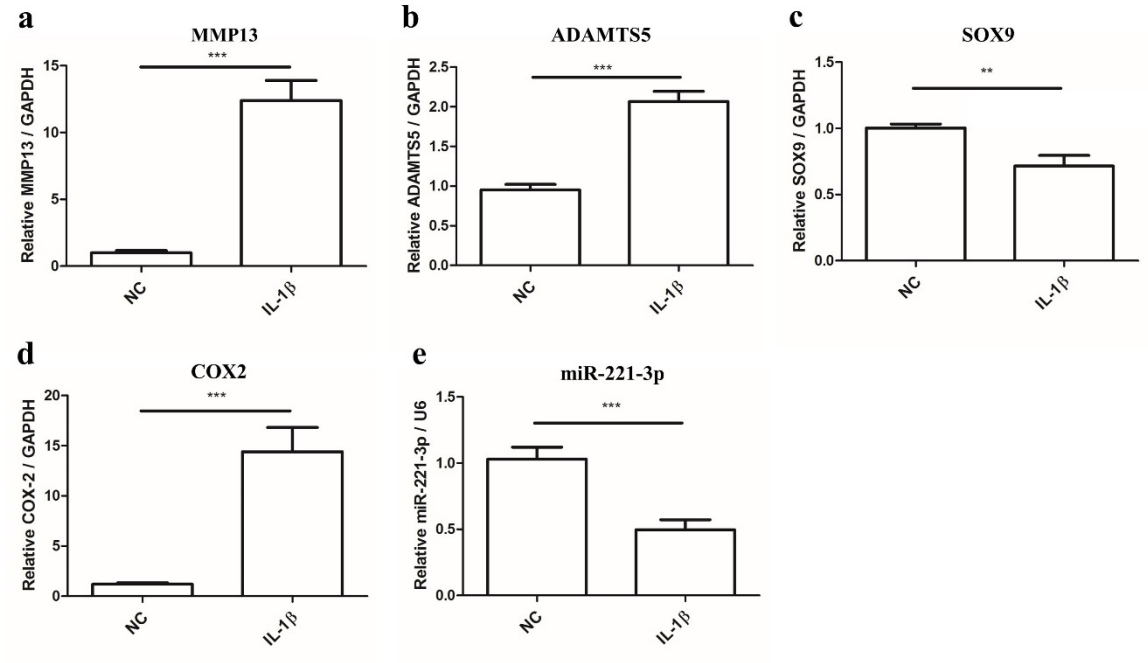

Figure 12: Relative gene expression in IL-1β treated chondrocytes. *MMP13*, *ADAMTS5*, and *COX2* were upregulated in IL-1β treated chondrocytes vs. corresponding control, while *SOX9* and *miR-221-3p* were downregulated. *MMP13*, *ADAMTS5*, *SOX9*, and *COX2* relative to *GAPDH*, *miR-221-3p* relative to *U6*. ***P*<0.01 and ****P*<0.001 vs. corresponding control.

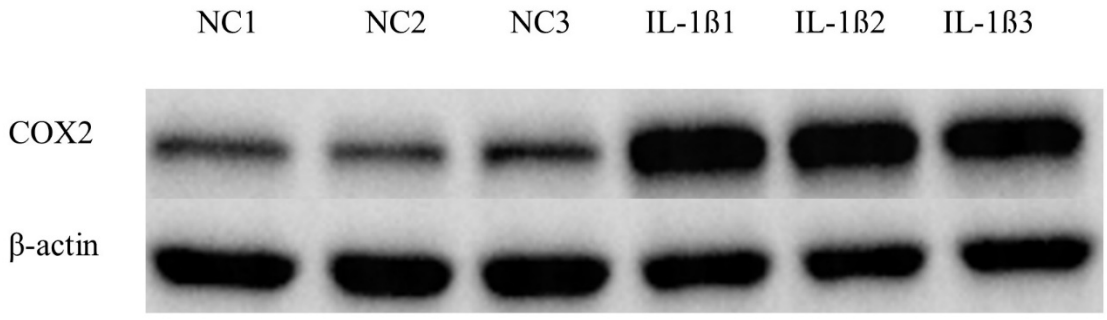

Figure 13: Relative COX2 expression in IL-1β treated chondrocytes. COX2 expression was increased in IL-1β treated chondrocytes vs. corresponding control. Relative to β-actin.

3.4. Effects of *miR-221-3p* on chondrocytes

To analyze the effect of *miR-221-3p* on chondrocytes, the cells were transfected with *miR-221-3p* mimic or scrambled control, and transfection efficiency was tested by qRT-PCR (Figure 14). The results showed 3μl *miR-221-3p* mimic （50 nM） would be the optimal concentration for the following experiment.

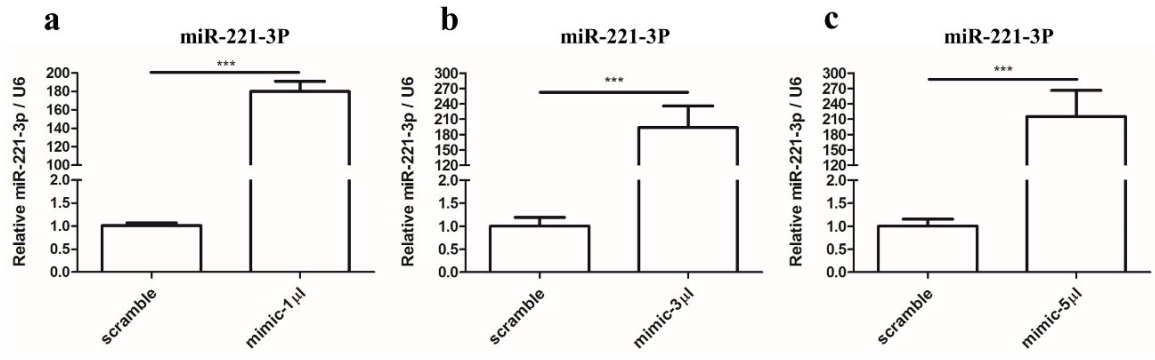

Figure 14: Transfection efficiency of *miR-221-3p* mimic was confirmed by qRT-PCR. Chondrocytes were transfected with 1 μl, 3 μl, and 3 μl *miR-221-3p* mimic and the corresponding control respectively for 48 hours. Relative to *U6*. ***P<0.001 vs. corresponding scrambled control.

At the same time, the expression of target genes was also analyzed by qRT-PCR, and the predicted targets including Cyclin-dependent kinase inhibitor 1B (*CDKN1B/p27*), Aryl Hydrocarbon Receptor Nuclear Translocator (*ARNT*), Tissue inhibitor of metalloproteinase 3 (*TIMP3*), Transcription factor 7-like 2 (*Tcf7l2/TCF4*), and *RUNX2* were significantly suppressed in the *miR-221-3p* mimic transfection group compared to the scrambled control (Figure 15).

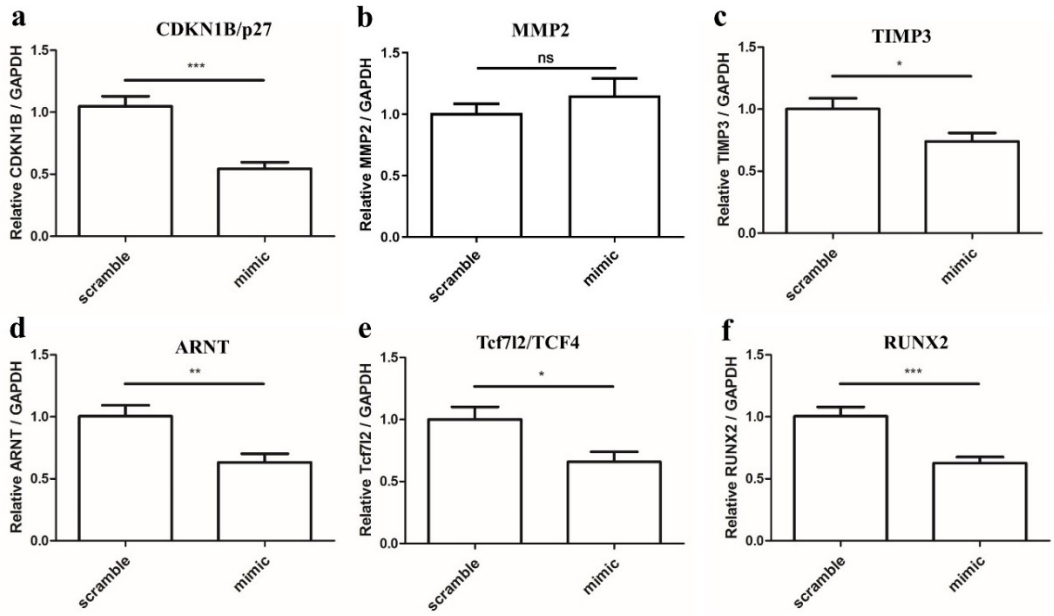

Figure 15: Relative expression of predicted targets of *miR-221-3p* in chondrocytes. Chondrocytes were transfected with scrambled control and *miR-221-3p* mimic, the expression level of predicted targets (a) *CDKN1B (p27)*, (c) *TIMP3*, (d) *ARNT*, (e) *Tcf7l2 (TCF4)*, and (f) *RUNX2* were significantly inhibited except (b) *MMP2*. Relative to *GAPDH*, ns stands for not statistically significant, **P*<0.05, ***P*<0.01, and ****P*<0.001 vs. corresponding control.

Furthermore, *miR-221-3p* mimic transfection was able to significantly increase the expression of vascular endothelial growth factor B (*VEGFB*) in chondrocytes when compared with scrambled control. While the expression *MMP13* and *ADAMTS5* were significantly decreased. Based on the results of the cell proliferation experiment, it was concluded that *miR-221-3p* could promote the proliferation of chondrocytes *in vitro* compared to the scrambled control, although the result was not statistically significant. These results indicated that overexpression of *miR-221-3p* in chondrocytes maybe promote angiogenesis and proliferation in cartilage and play a protective role in chondrocyte degeneration (Figure 16).

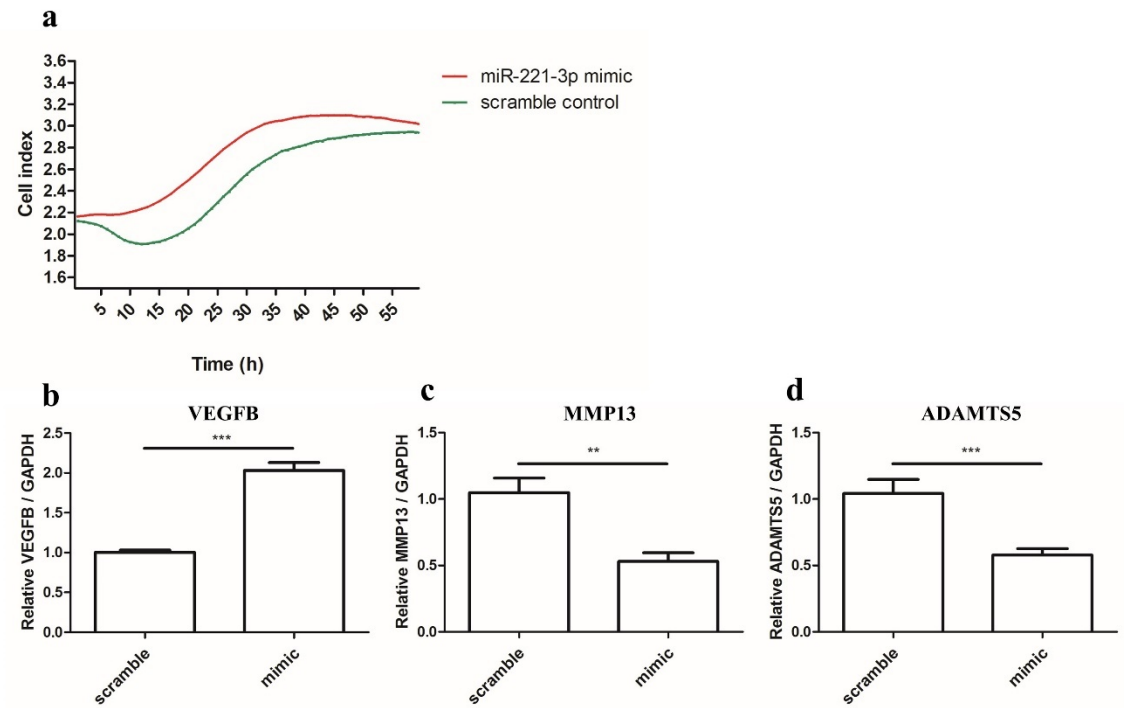

Figure 16: Effect of *miR-221-3p* on chondrocytes. Chondrocytes were transfected with *miR-221-3p* mimic and scrambled control, proliferation ratio was detected by xCelligence (a). The expression level of *VEGFB* (b) and catabolic genes *MMP13* (c), *ADAMTS5* (d) were measured by qRT-PCR. Relative to GAPDH. **P<0.01 and ***P<0.001 vs. corresponding control.

3.5. Chondrocyte-osteoblast communication

We firstly investigated whether chondrocytes transfected with *miR-221-3p* could affect the bone formation capacity of osteoblasts through coculture in transwell plates. According to the qRT-PCR results, the *miR-221-3p* expression level was increased in osteoblasts cocultured with chondrocytes transfected *miR-221-3p* mimic compared to the scrambled control (Figure 17a, c). Subsequently, we isolated EVs from cocultured medium, and a significant upregulation of *miR-221-3p* was expressed in the EVs of the *miR-221-3p* mimic group compared to the scrambled control (Figure 17b).

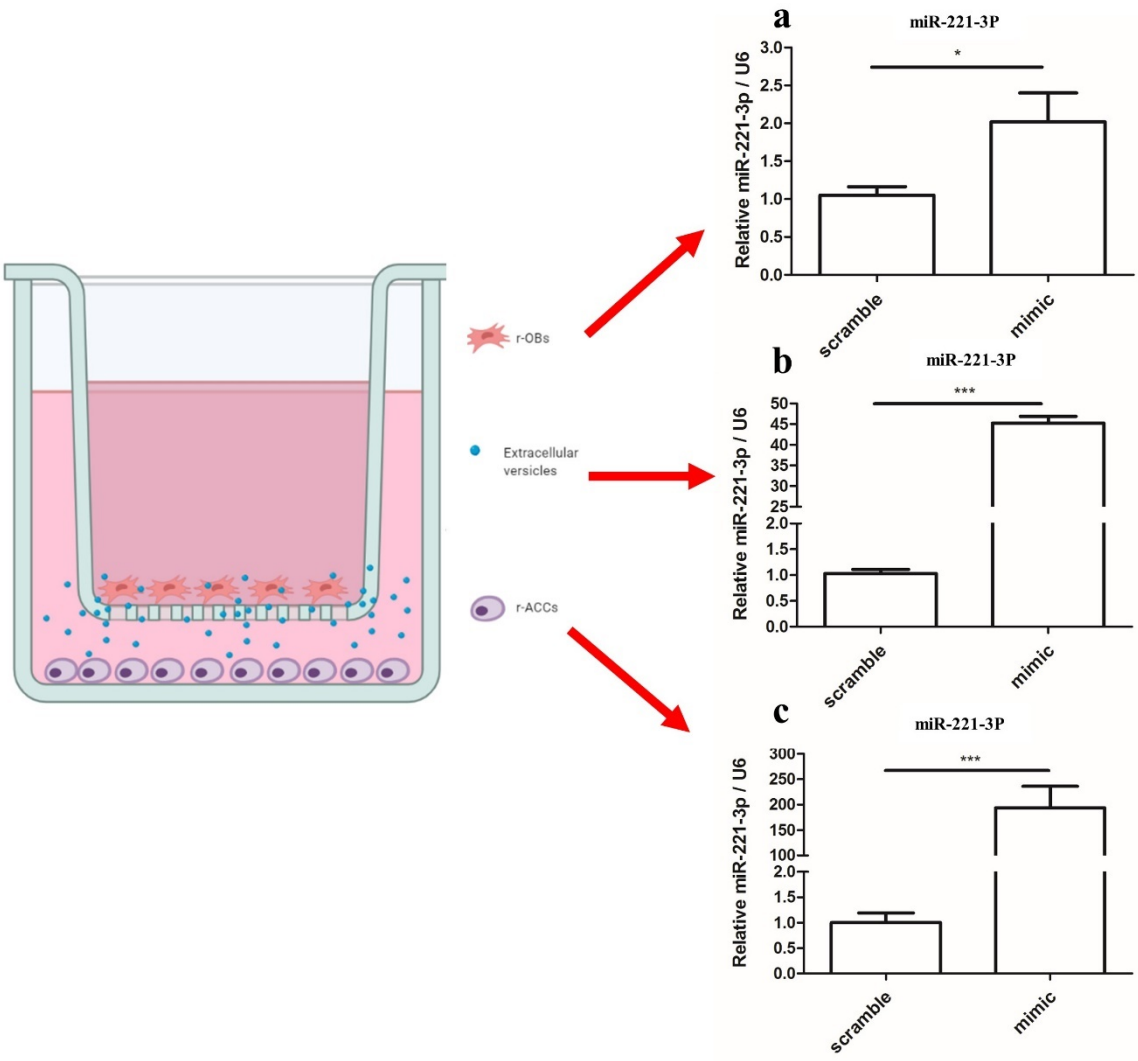

Figure 17: The relative expression of *miR-221-3p* in the cocultured chondrocytes and osteoblasts, and EVs. (a) *MiR-221-3p* concentration can be increased by transfection in chondrocytes. (b) EVs were isolated and checked for *miR-221-3p* concentration. (c) *MiR-221-3p* expression in osteoblasts was increased significantly by *miR-221-3p* loaded EVs. *miR-221-3p* relative *U6*, **P*<0.05 and ****P*<0.001 vs. corresponding control.

Meanwhile, the expression of related targets of *miR-221-3p* in osteoclasts was significantly decreased (Figure 18a-d). Moreover, chondrocytes transfected with *miR-221-3p* inhibited osteogenic markers of osteoblasts compared with the scrambled control, and main osteogenic markers such as *COL1A1* and *RUNX2* were decreased while the expression of *OCN* was not changed (Figure 18e-g).

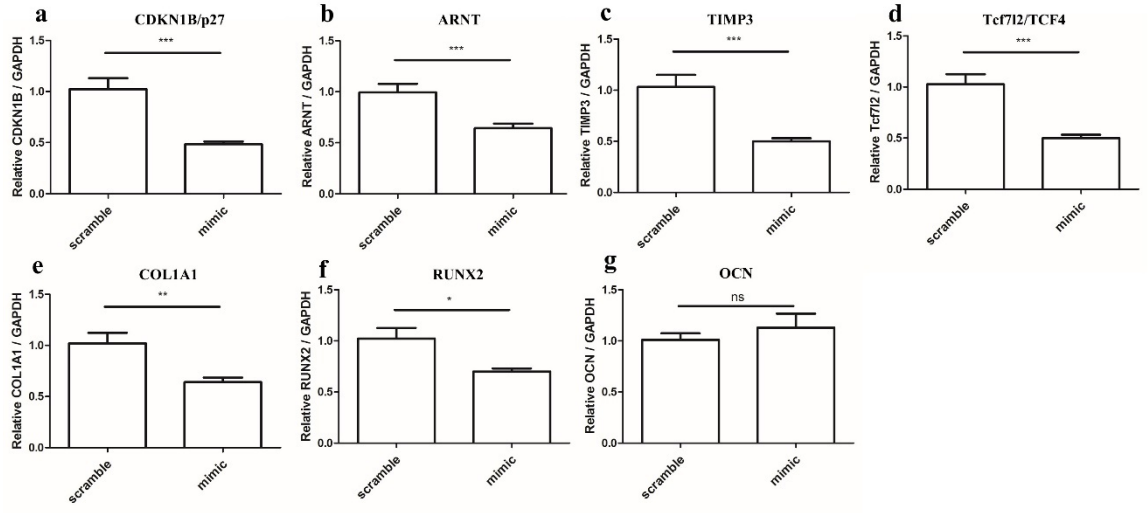

Figure 18: Relative gene expression in cocultured osteoblasts. The expression level of *COL1A1*, *RUNX2*, and the targets of *miR-221-3p, CDKN1B/p27*, *ARNT*, *TIMP3*, and *Tcf7l2/TCF4* in osteoblasts cocultured with chondrocytes transfected with *miR-221-3p* mimic were significantly decreased compared with a scrambled control, while mir-221-3p was upregulated. (a) *CDKN1B/p27*, (b) *ARNT*, (c) *TIMP3*, (d) *Tcf7l2/TCF4*, (e) *COL1A1*, (f) *RUNX2*, (g) *OCN* relative to *GAPDH*, *miR-221-3p* relative to *U6*. ns stands for not statistically significant, **P*<0.05, ***P*<0.01, and ****P*<0.001 vs. corresponding control.

3.6. Effect of *miR-221-3p* on osteoblasts

After 2 weeks' osteogenic differentiation, *miR-221-3p* expression was decreased without statistical significance in the osteoblasts of the negative control group compared to the blank control group, while the osteogenic markers *RUNX2* and *OCN* were increased significantly except for *COL1A1* (Figure 19).

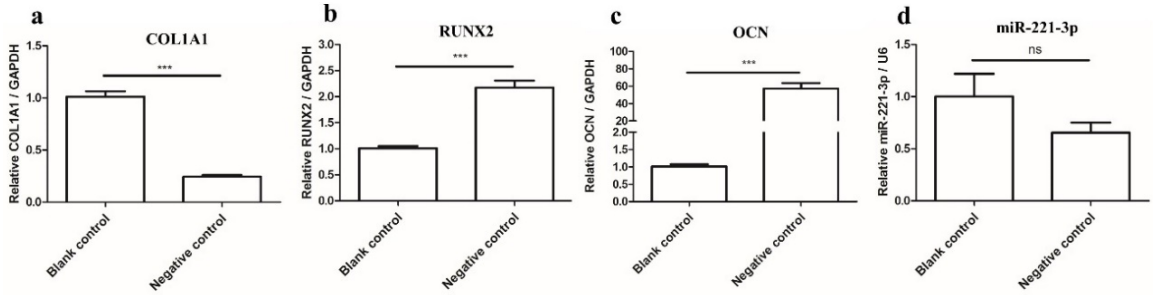

Figure 19: Relative expression of osteogenic markers and *miR-221-3p* in osteoblasts after 2 weeks of osteogenic differentiation. Negative control was cultured with ODM and

blank control was cultured with BM. The expression level of (a) *COL1A1* were downregulated, while osteogenic markers (b) *RUNX2*, (c) *OCN* were upregulated after 2 weeks of osteogenic differentiation. (d) *miR-221-3p* expression was also decreased without statistical significance. *COL1A1*, *RUNX2*, *OCN* relative to *GAPDH*, *miR-221-3p* relative to *U6*. ns stands for not statistically significant, ***P<0.001 vs. corresponding control. BM=Basal medium, ODM=Osteogenic differentiation medium.

To understand the effect of *miR-221-3p* in osteoblasts, we performed 2 weeks' osteogenic experiments with osteoblasts which were transfected with *miR-221-3p* mimic and scrambled control at 1st day, 4th day, 7th day, 10th day respectively, and harvested on the 14th day. Transfection efficiency, the expression level of targets, and osteogenic markers were measured by qRT-PCR. As shown, *miR-221-3p* expression was successfully increased in the *miR-221-3p* mimic transfected cells compared to scrambled control, and the targets of *miR-221-3p* were all significantly decreased (Figure 20d and Figure 21). Compared with the scrambled control cells, osteogenic markers such as *COL1A1*, *RUNX2*, and *OCN* were significantly diminished in the mimic transfected cells (Figure 20a-c).

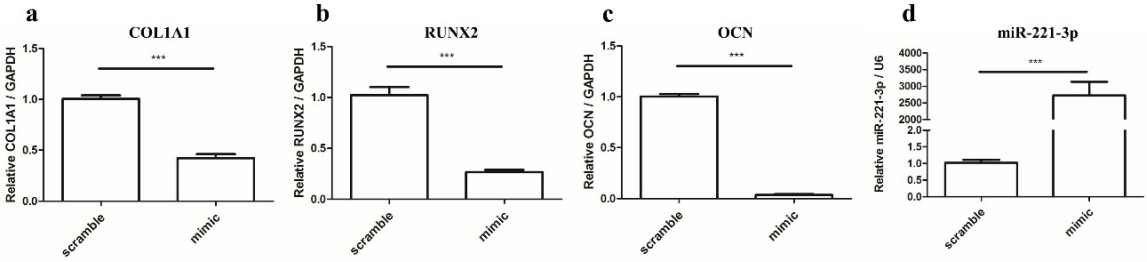

Figure 20: Relative expression of osteogenic markers and *miR-221-3p* in osteoblasts transfected with *miR-221-3p* mimic after 2 weeks of osteogenic differentiation. Osteoblasts transfected with scrambled control and *miR-221-3p* mimic were cultured with ODM for 2 weeks, the expression level of osteogenic markers (a) *COL1A1*, (b) *RUNX2*, (c) *OCN* was inhibited significantly, and (d) *miR-221-3p* was increased. *COL1A1*, *RUNX2*, *OCN* relative to *GAPDH*, *miR-221-3p* relative to *U6*. ***P<0.001 vs. corresponding control. ODM=Osteogenic differentiation medium.

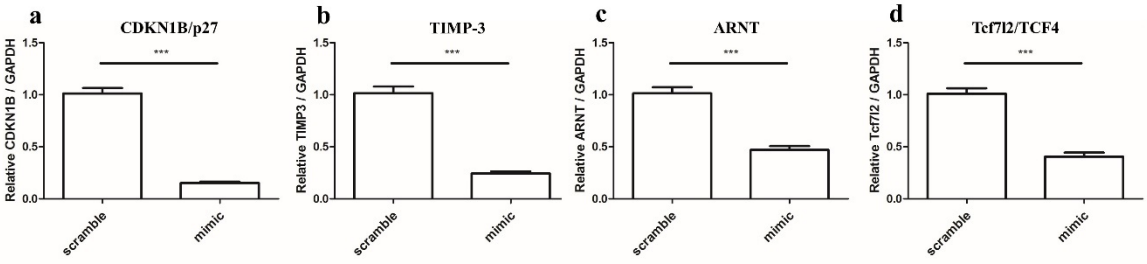

Figure 21: Relative gene expression in osteoblasts transfected with *miR-221-3p* mimic after 2 weeks of osteogenic differentiation. Osteoblasts transfected with scrambled control and *miR-221-3p* mimic were cultured with ODM for 2 weeks, the expression of

predicted targets (a) *CDKN1B/p27*, (b) *TIMP3*, (c) *ARNT*, and (d) *Tcf7l2/TCF4* was inhibited significantly. Relative to *GAPDH*, ns stands for not statistically significant. ***$P<0.001$ vs. corresponding control.

Von Kossa staining and Alizarin red staining were performed to evaluate the bone formation potential of osteoblasts and indicated its significant inhibition by *miR-221-3p* versus scrambled control (Figure 22 and Figure 23).

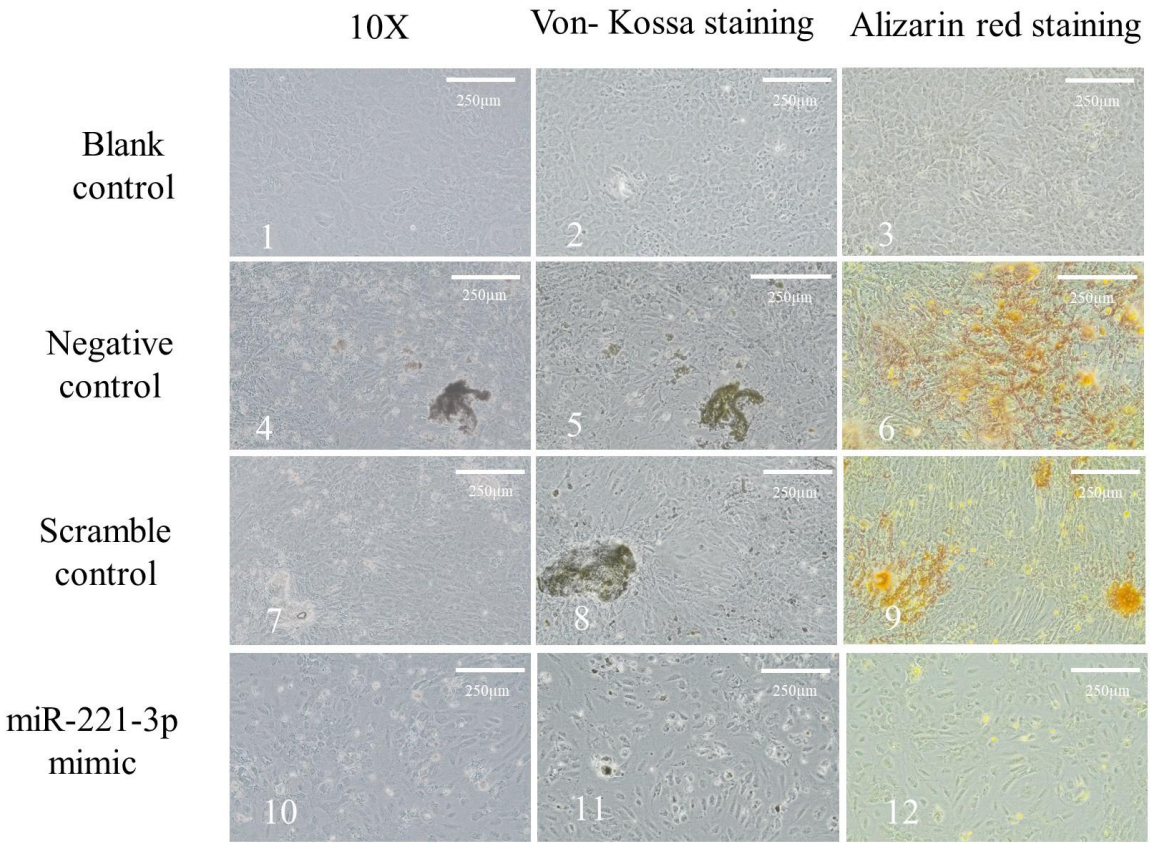

Figure 22: Microscopic images of staining results after 2weeks' culture in different conditions. Mineralized nodule formation of osteoblasts was illustrated by Von Kossa staining and Alizarin red staining after 2weeks' culture in different conditions. *miR-221-3p* mimic (10,11,12), scrambled control (7,8,9) and negative control (4,5,6) groups were cultured in ODM. The blank control (1,2,3) group was cultured with BM.

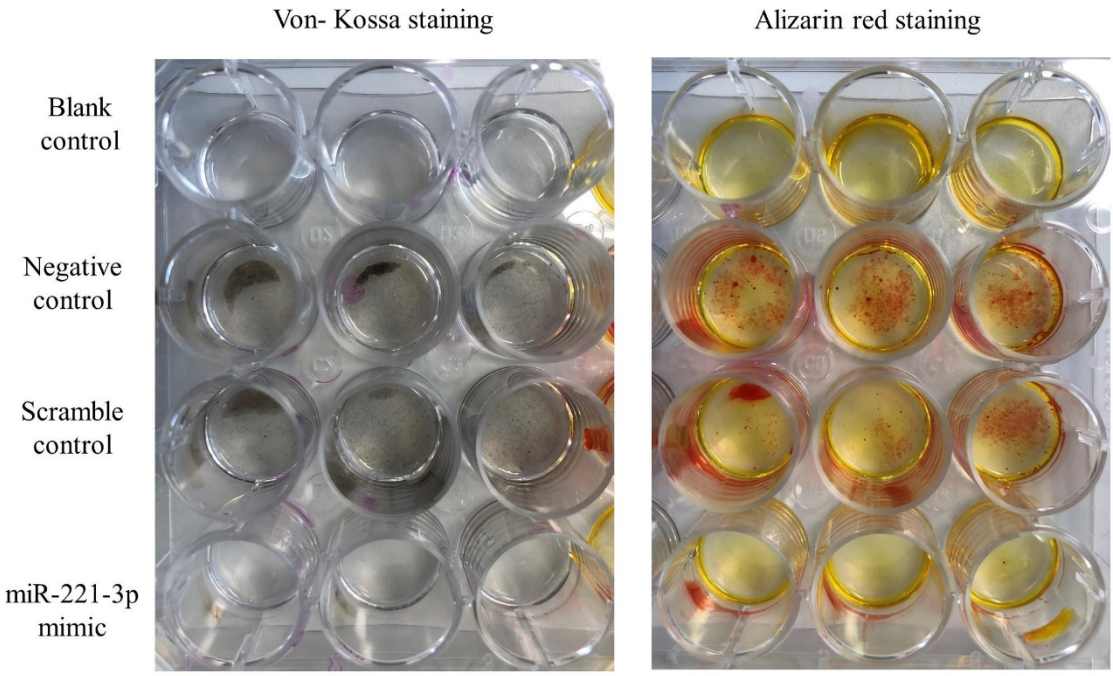

Figure 23: Macroscopic images of the staining results after 2weeks' culture in different conditions. *MiR-221-3p* mimic, scrambled control and negative control groups were cultured in ODM. The blank control group was cultured with BM.

3.7. *MiR-221-3p* loaded EVs inhibits the osteogenic capacity of osteoblasts

To determine the effect of *miR-221-3p* loaded EVs on osteoblast function, we treated osteoblast with chondrocytes secreted EVs modified with *miR-221-3p* mimic or scrambled control at a concentration of 1.0 x 10^8 particles/well (Figure 24), 1.0 x 10^9 particles/well (Figure 25 and Figure 26), 1.0 x 10^{10} particles/well (Figure 27) respectively. The result demonstrated that *miR-221-3p* loaded EVs with the concentration of 1.0 x 10^9 particles/well significantly inhibited the mRNA expression levels of *COL1A1*, *RUNX2*, *OCN*, and targets of *miR-221-3p* in osteoblasts. These data indicate that rACCs-derived *miR-221-3p* loaded EVs may inhibit the osteogenic capacity of osteoblasts.

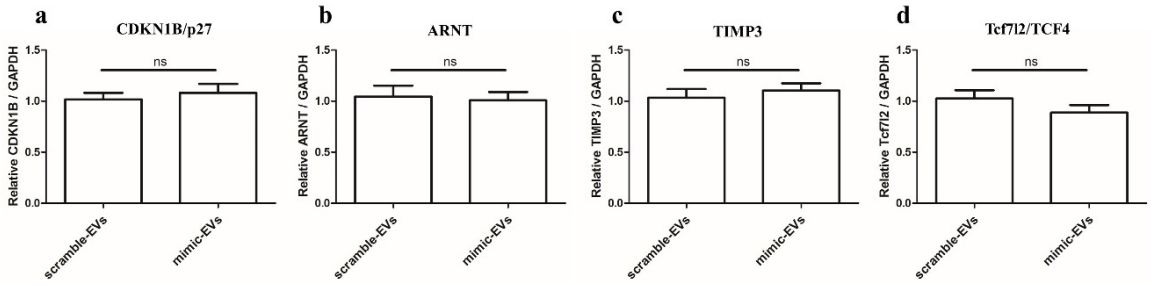

Figure 24: Relative gene expression in osteoblasts cocultured with *miR-221-3p* modified EVs (1.0 x 10^8 particles/well) for 48 hours. Expression level of (a) *CDKN1B/p27*, (b) *ARNT*, (c) *TIMP3* and (d) *Tcf7l2/TCF4* in osteoblasts cocultured with *miR-221-3p* modified EVs (1.0 x 10^8 particles/well) for 48hours didn't show significant difference vs. corresponding scrambled control loaded EVs. Relative to *GAPDH*. ***P<0.001 vs. corresponding control.

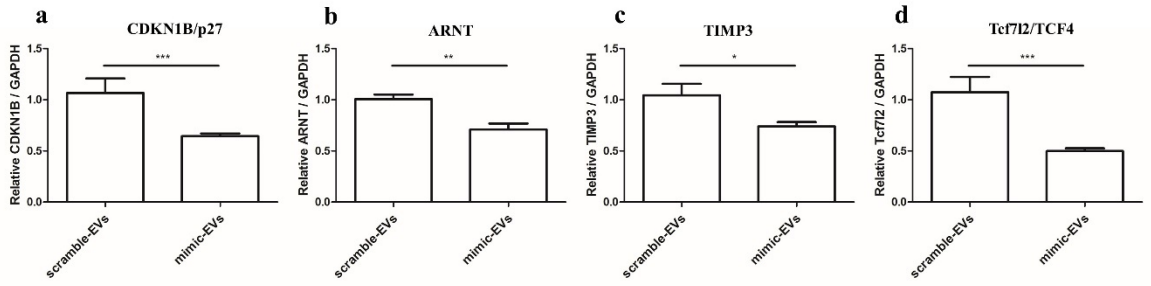

Figure 25: Relative gene expression in osteoblasts cocultured with *miR-221-3p* modified EVs (1.0 x 10^9 particles/well) for 48 hours. Expression level of (a) *CDKN1B/p27*, (b) *ARNT*, (c) *TIMP3* and (d) *Tcf7l2/TCF4* in osteoblasts cocultured with *miR-221-3p* modified EVs (1.0 x 10^9 particles/well) for 48 hours were significantly decreased vs. corresponding control loaded EVs. Relative to *GAPDH*. ***P<0.001 vs. corresponding control.

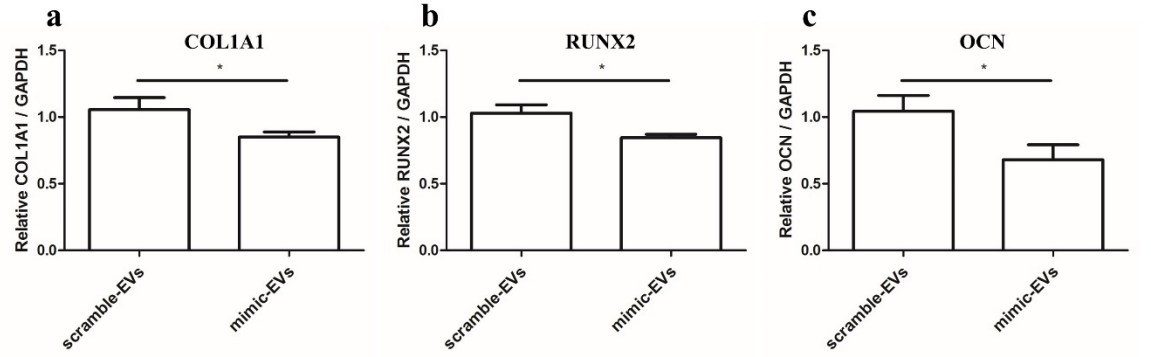

Figure 26: Relative gene expression in osteoblasts cocultured with *miR-221-3p* modified EVs (1.0 x 10^9 particles/well) for 48 hours. The expression level of (a) *COL1A1*, (b) *RUNX2*, and (c) *OCN* in osteoblasts cocultured with *miR-221-3p* modified EVs (1.0 x

10^9 particles/well) for 48 hours were significantly decreased vs. corresponding control miRNA loaded EVs. Relative to *GAPDH*. ***P<0.001 vs. corresponding control.

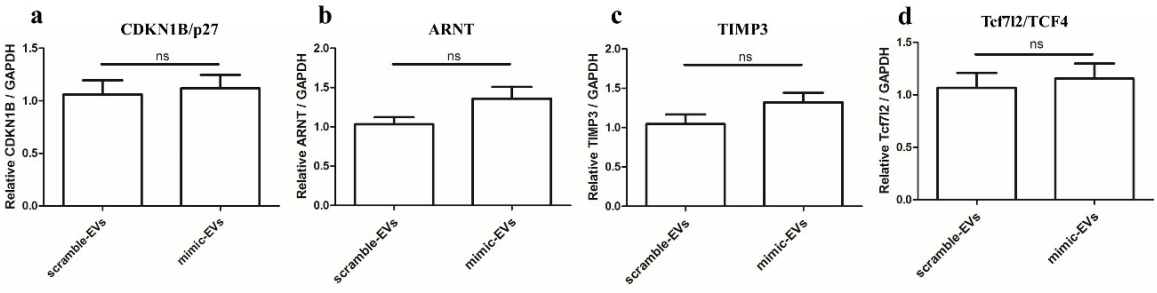

Figure 27: Relative gene expression in osteoblasts cocultured with *miR-221-3p* modified EVs (1.0 x 10^{10} particles/well) for 48 hours. Expression level of (a) *CDKN1B/p27*, (b) *ARNT*, (c) *TIMP3*, and (d) *Tcf7l2/TCF4* in osteoblasts cocultured with *miR-221-3p* modified EVs (1.0 x 10^{10} particles/well) for 48 hours didn't show significantly difference vs. corresponding scramble control miRNA loaded EVs. Relative to *GAPDH*. ***P<0.001 vs. corresponding control.

4. Discussion

4.1. Cell source, identification of cells, and establishment of OA model *in vitro*

To research the chondrocyte-osteoblast communication *in vitro*, there are three cell sources to choose from: human chondrocytes and osteoblasts, animal chondrocytes and osteoblasts, and MSCs. Human cells can be the optimal choice for scientific research considering that the results are more reliable with no species differences (Chu et al. 2010). However, for ethical reasons, only a limited number of cells can be obtained from patients. More importantly, the chondrocytes isolated from patients can be hypertrophic and senescent due to the long-time influence of the disease environment. As for animal cells, the commonly used is the rodent system, for example, rats and mice. Although it is easier to obtain large amounts of cells from animals compared to humans, the species differences between animals and humans and may affect the clinical transformation of experimental results. With the development of tissue engineering, the technology to differentiate MSCs derived from diverse sources into chondrocytes and osteoblasts has matured (Andrzejewska et al. 2019). However, although the marker genes such as *COL2*, *SOX9,* and Aggrecan *(AGG)* for chondrocytes, and *COL1A1*, *RUNX2,* and *OCN* for osteoblasts can be positively expressed in differentiated MSCs, these cells can't replace the real chondrocytes and osteoblasts, given the different cultural environment *in vitro* compared to the growth environment *in vivo* (Bernstein et al. 2010). The rat was selected as the cell source for the present study. Except for the advantage of easy access compared to human cells, rats are larger and easier to manipulate compared to mice. In addition, I already have the experience to isolate and culture chondrocytes and chondrocytes from the rat (Wang et al. 2018).

As the main constituent of the cartilage matrix, the expression of COL2 is the typical characteristic of chondrocytes (Marlovits et al. 2004). Therefore, COL2 was selected as the protein marker to identify the isolated chondrocytes and the IF result showed a remarkably positive COL2 IF signal. Besides, the typical "cobblestone" morphology was another evidence to testify to the chondrocytes (Karim et al. 2018). To identify osteoblasts, the cells were treated with the ODM containing β-Glycerophosphate disodium salt hydrate and L-Ascorbic acid 2-phosphate. The results demonstrated a positive von Kossa and Alizarin red staining after 2 or 3 weeks' culture, although there was no obvious difference between these two time points. Meanwhile, qRT-PCR also supported the staining results and all the osteogenic markers *COL1A1*, *RUNX2*, and *OCN* were upregulated after 2 weeks'

osteogenic differentiation. Moreover, the effect of ODM with and without Dexa was compared on the osteogenic capacity of osteoblasts. As expected, Dexa significantly inhibited the bone formation capacity of osteoblasts after 2 weeks' culture based on the staining and qRT-PCR results and this conclusion was consistent with previous reports (Iu et al. 2005; Pan et al. 2019). Although this result was easy to be understood and accepted due to the viewpoint of glucocorticoid-induced osteoporosis (Seibel et al. 2013), the inhibited effect of Dexa on mineralization and the osteoblastic gene expressions in osteoblasts was contradictory with the previous conclusion that Dexa could promote osteoblast differentiation and matrix mineralization (Shalhoub et al. 1992; Eijken et al. 2006; Mikami et al. 2007). The possible explanation for the paradoxes can be that the additional dose of Dexa may induce complex effects depending on the specific environment, for example, different cell lines, the distinguished composition of the medium, and the duration of the differentiation.

To clarify the *miR-221-3p* expression in OA chondrocytes, *in vitro* OA model was established with IL-1β treated chondrocytes according to previous experience (Wang et al. 2018). The relevant gene and protein expression in the OA model was tested by qRT-PCR and western blot analysis. The results showed catabolic genes *MMP13* and *ADAMTS5* were upregulated and anabolic gene *SOX9* was downregulated significantly. Further, both mRNA and protein levels of the inflammatory factor *COX2* were remarkably increased. This data indicated a successful OA model *in vitro* and the *miR-221-3p* expression was detected to be downregulated in OA chondrocytes and this result was consistent with a previous study (Zheng et al. 2017).

4.2. Feasibility of communication between cartilage and subchondral bone

This study aimed to research the specific role of EV-mediated *miR-221-3p* in the communication of chondrocytes and osteoblasts. Recent studies have demonstrated the possibility of bone-cartilage communication through various microchannels, such as vascular channels and microcracks (Taheri et al. 2019; Taheri et al. 2021). For example, Pan et al demonstrated that sodium fluorescein could be transferred between the bone marrow and the articular space in mouse joints, which was direct evidence of interaction between the subchondral bone and articular cartilage (Pan et al. 2009). Several studies even suggested subchondral plate was with increased porosity in OA patients compared with healthy control, which could promote the interaction between the bone and cartilage compartments (Botter

et al. 2011; Iijima et al. 2016). In this study, it was found the osteoblasts showed an upregulated expression of *mi*R-*221-3p* and this can be caused by the cocultured chondrocytes pre-transfected with the *mi*R-*221-3p* mimic in a vitro co-culture model. Furthermore, the EVs isolated from the supernatant of chondrocytes were demonstrated to contain the *mi*R-*221-3p*. This opens the possibility of *mi*R-*221-3p* transportation via EVs between chondrocytes and osteoblasts, which was also indirect evidence of communication at the cartilage-bone interface. Similarly, Sanchez et al isolated osteoblasts from sclerotic or non-sclerotic regions of the subchondral bone in human patients with knee OA and chondrocytes from the healthy articular knee cartilage and thereafter cocultured in alginate beads. Results demonstrated that sclerotic osteoblasts could deteriorate cartilage degradation by inducing chondrocytes to produce more catabolic enzymes such as matrix metalloproteinases (MMPs) and reducing AGG synthesis compared with chondrocytes cultured alone (Sanchez et al. 2005). Altogether, current results indicated the feasibility of communication between chondrocytes and osteoblasts via the EVs and this is the premise of this experiment.

4.3. *MiR-221-3p* in the pathogenesis of OA

Previous studies have reported the role of *mi*R-*221* in different fields, especially in various kinds of malignant cancers such as breast cancer, liver cancer, and bladder cancer (Song et al. 2019). For example, *mi*R-*221* was demonstrated to target cyclin-dependent kinase inhibitors *p27* and *p57* in both mRNA and protein levels and promote the malignant proliferation of glioblastoma cells (Medina et al. 2008). However, different from malignant cancers, osteoarthritis is a chronic inflammatory disease caused by wear and stress stimulation and *mi*R-*221* might play a different role by targeting corresponding targets. In this study, the expression of *mi*R-*221-3p* was demonstrated to be downregulated in IL-1β treated chondrocytes and transfected chondrocytes with *mi*R-*221-3p* mimic could significantly inhibit the expression of *MMP13* and *ADAMTS5*. This is consistent with previous reports (Zheng et al. 2017). Except for the anti-inflammatory action in OA, *mi*R-*221* has also been used in the regeneration field to promote chondrogenic differentiation from MSCs to treat cartilage defects in OA. Lolli et al found *mi*R-*221* expression showed a dynamic process of change from MSCs to differentiated chondrocytes, and then de-differentiated chondrocytes. In brief, *mi*R-*221* expression decreased during TGFβ-driven chondrogenesis from MSCs while increasing during the de-differentiation process from chondrocytes. To prove *mi*R-*221* could regulate chondrogenesis negatively, this group used *antagomi*R-*221* to drive the chondrogenic differentiation of MSCs in a conventional 2D

method which was less effective than the 3D pellet method. However, after 2 weeks of differentiation without TGFβ treatment, the MSCs exposed to *antagomiR-221* decreased the protein expression levels of COL1, while increased the expression of COL2 and SOX9 in a time-dependent manner (Lolli et al. 2014). This result indicated that *miR-221* might be a hopeful target for cartilage regeneration.

MiR-221 was reported to regulate cancer development by promoting proliferation, migration, invasion, and metastasis of tumor cells (Song et al. 2019). In the present study, *miR-221-3p* was also shown to promote the proliferation of chondrocytes base on the result of xCELLigence although the result was not statistically different. The potential explanation was that *miR-221-3p* could inhibit the expression of *CDKN1B/p27*. Similarly, Wang et al also showed that EVs containing *miR-221-3p* could promote chondrocyte proliferation versus the corresponding control by using CCK-8 assay, while the exact mechanism was not further reported (Wang et al. 2020).

MiR-221 is special due to its mechanosensitive characteristic and its expression in cartilage can be modulated by mechanical loading. For example, Dunn et al found *miR-221* expression was up-regulated in bovine articular cartilage bearing greater weight stress (Dunn et al. 2009). Recently, Hecht et al compared the miRNA expression profiles in human chondrocytes under "beneficial" and "non-beneficial" loading regimes and *miR-221* was found to be increased in both of these two distinct loading modes compared to the unloaded control (Hecht et al. 2019). Osteoarthritis has been generally regarded as a whole joint disease with the crucial feature of abnormal bone and cartilage remodeling under daily mechanical loading instead of a simple result of wear and tear (Loeser et al. 2012). Although mechanical transduction from cartilage to the subchondral bone plays an indispensable role in the remodeling process of subchondral bone, the exact mechanism of how the biological signals induced by mechanical stress in cartilage are transferred to subchondral bone is still to be elucidated.

Interestingly, the present study identified five potential targets of *miR-221-3p* through three public databases, namely *CDKN1B/p27*, *TIMP3*, *ARNT*, *RUNX2* and *TCF4*. All these genes were downregulated in *miR-221-3p* overexpressed chondrocytes and osteoblasts. As mentioned above, *CDKN1B/p27* is an inhibitor of cyclin-dependent kinase and *miR-221-3p* could inhibit its expression in chondrocytes and further promote chondrocyte proliferation. It was also reported *CDKN1B/p27* could be active in osteoblasts and osteosarcoma cell lines (Hu et al. 2019). As a result, *miR-221-3p* can be a promising target to modulate the proliferation of osteoblasts and further affect osteoblast mediated bone formation.

TIMP3 is a member of the tissue inhibitor of the metalloproteinases family and is well known to inhibit the expression of various MMPs, which could further affect extracellular matrix (ECM) remodeling (Nakamura et al. 2020). More importantly, TIMP3 was initially found as a tumor suppressor and also a possible inhibitor of angiogenesis with or without MMPs inhibition. Meanwhile, it was also identified as a direct target of *miR-221* in various cancer cells (Gan et al. 2014; Zhang et al. 2015). Recently, TIMP3 was found to interact with vascular endothelial growth factor receptor 2 directly, a process through which TIMP3 could exert its antiangiogenic effect (Qi und Anand-Apte 2015). In the present experiment, it was also found that both chondrocytes and osteoblasts transfected with *miR-221-3p* mimic expressed more *VEGFB* compared with control, and this might provide another explanation for the angiogenesis effect of *miR-221-3p*. Moreover, Poulet et al establishment a transgenic mouse line by using the *Col2a1*-chondrocyte promoter, which could overexpress TIMP3 in chondrocytes. The overexpression of TIMP3 in cartilage could compromise the tibial bone structure and mechanical properties, and this suggested TIMP3 might participate in the regulation of cartilage and bone via specific paracrine pathways (Poulet et al. 2016). Considering both MMPs induced ECM remodeling and VEGFR mediated angiogenesis can be affected by TIMP3, further research on this target of *miR-221-3p* would be helpful to understand the role of *miR-221-3p* in the remodeling of cartilage and subchondral bone.

RUNX2 is a transcription factor that plays a crucial role in the process of chondrocyte hypertrophy and terminal maturation as well as in osteoblast differentiation during endochondral bone formation (Komori 2018). Overexpression of RUNX2 could activate the expression of protein catabolic enzymes, such as MMP13 and ADAMTS5 directly, or through participating in different singling pathways, for example, Wnt signal pathway and NF-$\varkappa$B pathway (Dong et al. 2006; Chen et al. 2012; Chern et al. 2020). The expression of RUNX2 was increased in OA cartilage, while the normal RUNX2 expression in healthy articular cartilage is minimal (Kamekura et al. 2005; Kamekura et al. 2006). In the present *in vitro* OA model, it was proven that *RUNX2* expression was significantly upregulated, while chondrocytes transfected with *miR-221-3p* mimic showed downregulation of *RUNX2*. At the same time, the osteoblasts cocultured with chondrocytes directly or EVs isolated from chondrocytes indirectly showed repressed osteogenic capability in the *miR-221-3p* mimic treated group. This result was consistent with previous studies that *miR-221* played an important part in osteogenic differentiation and bone formation by modulating *RUNX2* expression (Zhang et al. 2017). Therefore, *RUNX2* as a target of *miR-221-3p* can be a potential target for therapeutics of OA by preventing cartilage degradation and osteophyte formation. Although further studies are required due to its complex regulatory function.

Although most of the experiments *in vitro* so far have been completed in the incubator with normal oxygen levels (21%), most tissues and cells in our body live in a hypoxia environment depending on the specific route to receive oxygen from vessels(Pfander und Gelse 2007). Especially, the articular cartilage could only obtain oxygen from the synovial fluid directly and the microchannels of the subchondral bone indirectly, and is well known as hypoxic tissue due to the avascular nature (Treuhaft und MCCarty 1971; Kiaer et al. 1988). Previous studies have implicated hypoxia-inducible factors (HIFs) as the most important gene regulatory factors when facing hypoxic conditions (Qing et al. 2017). HIF-1 is known as a heterodimer consisting of HIF-1α and HIF-1β (Wang et al. 1995). Extensive evidence has demonstrated that HIF-1α is necessary to the survival of chondrocytes in cartilage, and its expression can be increased in OA joint due to less oxygen in the synovial fluids compared to healthy joint (Levick 1990; Biniecka et al. 2010). Meanwhile, it was found that HIF-1α can not only be modulated by hypoxia but also proinflammatory mediators and mechanical load in articular chondrocytes (Giatromanolaki et al. 2003; Coimbra et al. 2004).

However, compared to the ample studies and deep understanding of HIF-1α, another subunit HIF-1β, also called ARNT was less reported. In theory, the HIF-1α/ ARNT complex is the main regulator which is responsible for the adaptive responses to low oxygen tension. As a result, it is reasonable to consider ARNT as a putative treatment target while studying the HIF pathway (Chen et al. 2019). However, ARNT was thought of as constitutively expressed, and hypoxia-dependent upregulation of ARNT was much more like a cell-type-specific phenomenon (Mandl und Depping 2014). Besides, although Yuan et al found that miR-221 could affect hepatocyte proliferation by targeting *ARNT* which could further regulated p27 expression. The whole process was most likely independent of hypoxia (Yuan et al. 2013). In this study, *ARNT* was predicted and identified as a target of *miR-221-3p* and it was downregulated in cells transfected with *miR-221-3p* mimic. Given that the HIF pathway is related to various biological processes such as erythropoiesis (Krock et al. 2015), angiogenesis (Chen et al. 2016), and chondrocyte metabolism (Hwang et al. 2017), *miR-221-3p* might participate in the modulation of cartilage and bone remodeling by targeting *ARNT*. To understand the role of *ARNT* in the HIF pathway and OA pathogenesis, further research in a hypoxic environment is necessary on the mechanism of the hypoxia-dependent regulation of *ARNT*.

TCF4 also called tcf7l2, is well known for its participation in the modulation of the Wnt/β-catenin pathway (Bengoa-Vergniory und Kypta 2015). During the transduction of the Wnt/β-catenin pathway, Wnt–FZD interactions could prevent β-catenin from degradation,

and accumulated β-catenin in the cytoplasm will be translocated to the nucleus, where it stimulates downstream gene expression by combining the transcriptional complex TCF/LEF. As a result, miRNAs that could affect the mRNA level of *TCF/LEF* negatively may modulate the signal transduction of the Wnt pathway and further affect the metabolism of chondrocytes and synoviocytes which will aggravate the pathogenesis of OA. *MiR-221* was reported to modulate Wnt/β-catenin pathway by targeting *TCF4* directly and thus to enhance aggressiveness and triple-negative breast cancer (TNBC) properties of breast cancers (Liu et al. 2018). However, no studies reported the result of *miR-221* mediated *TCF4* inhibition in the OA field although a series of studies have demonstrated that the Wnt pathway participates in the process of chondrogenic and osteogenic differentiation during skeletal development. The Wnt pathway plays a vital role in the hypertrophic pathogenesis of chondrocytes, which is also an important pathological process in OA (Zhou et al. 2017). Present results showed the inhibition effect of *miR-221-3p* on the bone formation capacity of osteoblasts can be caused by the crucial role of TCF4 in the classical Wnt pathway (Wang et al. 2019).

Therefore, *miR-221-3p* might regulate the metabolism of bone and cartilage in the knee joint by inhibiting the aforementioned targets and thus affect the pathophysiology of OA.

4.4. *MiR-221-3p* loaded EVs in cell-cell communication

MiR-221-3p could participate in the regulation of chondrocytes and osteoblasts based on experimental results. In brief, chondrocytes transfected with *miR-221-3p* mimic for 48 hours could inhibit the expression of catabolic genes *MMP13* and *ADAMTS5*, promote chondrocyte proliferation and stimulate the expression of *VEGFB*, all of which tended to a protective role in chondrocytes. Meanwhile, osteoblasts transfected with *miR-221-3p* mimic for 2 weeks showed a significantly inhibited osteogenic capacity due to downregulated osteogenic markers *COL1A1*, *RUNX2,* and *OCN*. At the same time, the mineralized nodule formation of osteoblasts illustrated by Von Kossa and Alizarin red staining showed the same trend as the qRT-PCR results. According to our results, *miR-221-3p* was found to inhibit the targets *CDKN1B/p27*, *TIMP3*, *ARNT*, *RUNX2*, and *TCF4* in both chondrocytes and osteoblasts and these targets could partially explain the functional mechanism of *miR-221-3p*. However, as discussed above, *miR-221-3p* was mechanosensitive in cartilage (Hecht et al. 2019; Stadnik et al. 2021). More importantly, signal communication between bone and cartilage through microchannels crossing the bone-cartilage interface plays a vital role in OA pathogenesis (Taheri et al. 2021). Recently, miRNAs contained in the cargo of EVs, which

could inhibit the expression of target messenger RNA (mRNA) through the RNA-induced silencing complex (RISC) induced posttranscriptional repression, have been reported to participate in the intercellular signal transduction through a paracrine mechanism and thus affect the metabolism of recipient cells (Valadi et al. 2007; Bartel 2009; Tkach und Théry 2016). More importantly, the bilayer of EVs could protect miRNAs from RNase-induced degradation during the transportation process (Mause und Weber 2010). Hence, it is reasonable to speculate that chondrocytes could communicate with osteoblasts via miRNAs transported by EVs. The present study cocultured these two cell types in an *in vitro* model, and the results indicated a direct transfer of *miR-221-3p* loaded EVs to osteoblasts with inhibited osteogenic markers expression of *COL1A1* and *RUNX2*, while the *OCN* was not inhibited due to specific role as a late marker for bone formation (Boskey et al. 1985). As previously mentioned, the cargo of EVs contains not only various proteins but also diverse RNAs and DNA, during which, miRNAs mediated signal transduction aroused great interest in scientists (Bertoli et al. 2015). Therefore, EVs were isolated from the chondrocytes pre-transfected with *miR-221-3p* mimic and used to treat osteoblasts directly. The results showed inhibited bone formation capacity of osteoblasts after 48 hours' culture in ODM and the osteogenic markers *COL1A1*, *RUNX2,* and *OCN* were also significantly inhibited. At the same time, three concentration gradients of EVs for the experiment (10^8 particles/5.0 x 10^4 cells, 10^9 particles/5.0 x 10^4 cells, and 10^{10} particles/5.0 x 10^4 cells) were adopted respectively and it was intrigued to find only the middle concentration could inhibit the osteogenic markers, while too more or too few particles of EVs didn't show the same effect. The result caused by a lower concentration could be accepted because underdosing seems an ideal interpretation, while the result caused by the higher concentration is not easy to explain. Limited literature explained this concentration-dependent phenomenon as the "Bimodal dose-dependence effect" which is a known effect in pharmacology (Bettermann et al. 2001; Sverdlov 2012). Although many studies have focused on the role of EVs in delivering biological molecules to affect the recipient cells in different fields, so far, it is still not clear what should be the best ratio of EVs/recipient cells to mimic physiological conditions. One reason could be the various methods to determine the EVs concentrations. For example, protein content and vesicle number are the most commen methods to quantify the EVs. Meanwhile, the exact research models depending on the tissue and cell types may also affect the exact amount of EVs to induce significant biological effect. Besides, EVs contents could also be changed under different contexts which means EVs under the same concentration might cause a different effect on the recipient cells. All of above factors may cause the

difference in the dose of EVs used in different studies. Therefore, considering a specific experimental context, it is reasonable to find a suitable concentration for own experiments.

Previous studies have shown a protective role of *miR-221-3p* in OA cartilage as discussed above. However, most research just focused on cartilage and didn't consider the knee joint as a whole. For example, Zheng et al concluded that *miR-221-3p* was a novel potential therapeutic target for osteoarthritis only based on their research evidence of *miR-221-3p* in chondrocytes without considering subchondral bone or other tissues in knee joint (Zheng et al. 2017). OA is a wear and tear disease affected by long-time mechanical stress in essence and both cartilage and subchondral bone contribute to the conduction and dispersion of stress. Therefore, the communication of chondrocytes and osteoblasts in these two compartments plays a vital role in the initiation and progression of knee joint OA.

Based on the above results, we conclude that the bone formation capacity of osteoblasts could be regulated by the signal of *miR-221-3p* transferred by chondrocytes secreted EVs (Figure 28).

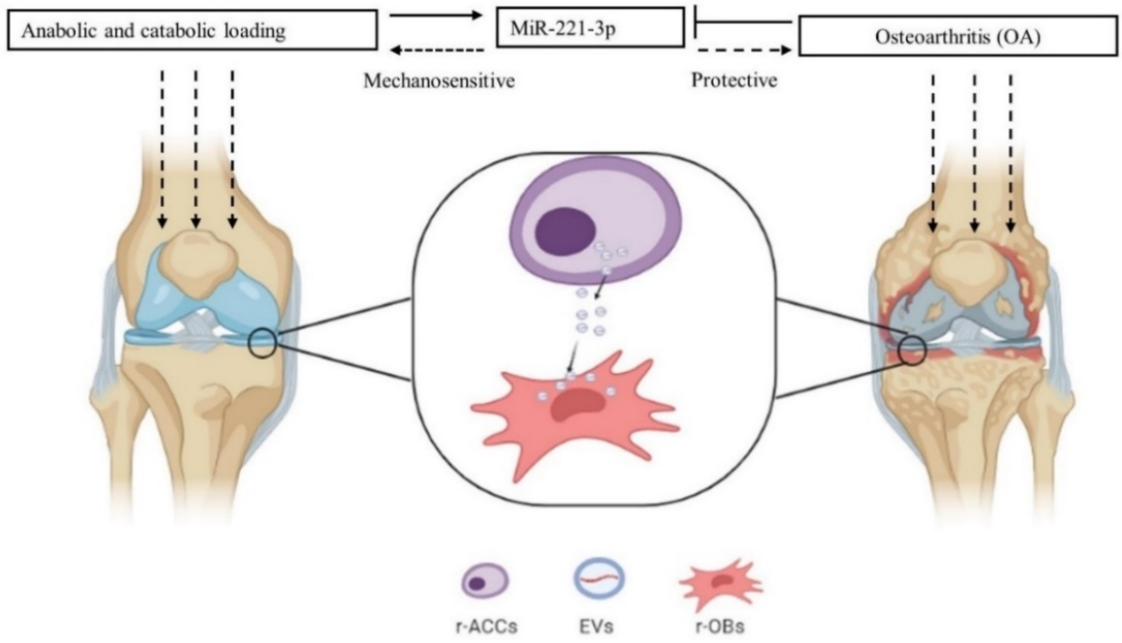

Figure 28: Schematic diagram of r-ACCs secreted EVs mediated by *miR-221-3p* affect r-OBs. Knee joint function is affected by mechanical stress. Articular cartilage destruction and subchondral bone sclerosis are hallmarks of OA and their interaction can play a crucial role in the initiation and progress of OA. The *miR-221-3p* expression can be regulated by both anabolic and catabolic loading. Meanwhile, *miR-221-3p* expression was demonstrated to be decreased in OA cartilage chondrocytes and abnormal *miR-221-3p* in chondrocytes may affect subchondral bone development through paracrine signals, such as EVs.

4.5. Limitations

There are also some limitations to this research. First of all, the mimic transfection method to overexpress *miR-221-3p* in chondrocytes can't fully simulate the real dynamic gene expression *in vivo,* so much more sophisticated methods would be required. Although we have predicated several targets through the online public databases, and test their expression by qRT-PCR, luciferase reporter assays would be necessary to identify the direct targets. Furthermore, a stable cell line overexpressing *miR-221-3p* would be ideal to obtain a constant expression and secretion of EVs. However, the cell line of chondrocytes always loss the biochemical characteristics compared to primary chondrocytes, especially the expression of COL2. Although present results demonstrated that *miR-221-3p* loaded EVs were involved in the communication between chondrocyte and osteoblasts *in vitro*, the detailed routes of how EVs are transferred across the cartilage-bone interface and the exact mechanism of how *miR-221-3p* inhibited the osteogenic capability of osteoblasts requires further exploration. Further studies are required to explore the effects of EVs mediated *miR 221-3p* in OA by affecting subchondral bone remodelling under mechanical loading *in vivo*. In the end, hundreds of miRNAs will participate in the regulation of joint homeostasis, and each miRNA also inhibits many different targets which will affect various signaling pathways at the same time. As a result, how to integrate the complex pathophysiological process into one simple approach would be crucial in future research.

5. Summary

Osteoarthritis is a whole joint disease manifested by cartilage degeneration and bone-cartilage communication plays a vital role in the disease progression. However, the knowledge of how the signal transduction from chondrocytes to osteoblasts happens is limited. Recently, *mi*R-*221-3p* was demonstrated to be mechanosensitive in cartilage chondrocytes and extracellular vesicles have been deeply researched for a specific role in cell-cell communication. This thesis aimed to investigate the putative role of *mi*R-*221-3p* modified extracellular vesicles in chondrocytes-osteoblasts communication. Chondrocytes and osteoblasts were isolated and identified from newborn rats. Then an *in vitro* osteoarthritis model was established with IL-1β treated chondrocytes. Catabolic genes including *MMP13, ADAMTS5, and COX2* were shown to be upregulated by qRT-PCR in IL-1β treated r-ACCs, while the anabolic gene *SOX9* was downregulated. Western blot analyses further confirmed that COX2 was overexpressed in the IL-1β treated chondrocytes. Meanwhile, *mi*R-*221-3p* expression was detected to be downregulated in this model. Furthermore, *mi*R-*221-3p* was overexpressed in chondrocytes through transfection with *mi*R-*221-3p* mimic and transfection efficiency was verified through inhibition level of various targets including *CDKN1B/p27, TIMP3, ARNT, RUNX2,* and *TCF4* by qRT-PCR. Subsequently, chondrocytes and osteoblasts were cocultured directly in the transwell for 48 hours to explore their communication *in vitro*. The qRT-PCR result demonstrated that *mi*R-*221-3p* overexpressed chondrocytes inhibited osteogenic markers of osteoblasts compared with the scrambled control. More importantly, the expression of *mi*R-*221-3p* was significantly increased in osteoblasts, while the relevant targets of *mi*R-*221-3p* were markedly decreased. To further explore the mechanism that how chondrocytes communicated with osteoblasts, extracellular vesicles were isolated from chondrocyte supernatant through PEG precipitation. Nanoparticle tracking analysis demonstrated that the size distribution of most extracellular vesicles ranged from 100 to 200 nm and characteristic marker CD81 was positively expressed in extracellular vesicles based on western blot analysis. Thereafter, osteoblasts were treated with extracellular vesicles isolated from chondrocytes modified with *mi*R-*221-3p* mimic or scrambled control for 48 hours, and the osteogenic capacity of osteoblasts was significantly inhibited. The results indicated a direct functional communication between chondrocyte and osteoblasts via extracellular vesicles. Therefore, this thesis gives some insight into the effect of *mi*R-*221-3p* in osteoblast-chondrocyte communication via extracellular vesicles. In conclusion, the study indicated that *mi*R-*221-3p* transferred by extracellular vesicles may be a novel regulator and play a vital role in the pathophysiological process of osteoarthritis.

APPENDIX

Xiaobin S, Böker KO, Taheri S, Lehmann W, Schilling AF (2021): Extracellular vesicles allow epigenetic mechanotransduction between chondrocytes and osteoblasts. Int J Mol Sci. 2021, 22,13282.

Xiaobin S, Böker KO, Taheri S, Hawellek T, Lehmann W, Schilling AF (2021): The Interaction between microRNAs and the Wnt/β-catenin Signaling Pathway in Osteoarthritis. Int J Mol Sci 22, 9887.

6. Reference

Alnahdi AH, Zeni JA, Snyder Mackler L (2012): Muscle impairments in patients with knee osteoarthritis. Sports Health 4, 284–292

Andreu Z, Yáñez-Mó M (2014): Tetraspanins in Extracellular Vesicle Formation and Function. Front Immunol 5, 442

Andrzejewska A, Lukomska B, Janowski M (2019): Concise Review: Mesenchymal Stem Cells: From Roots to Boost. Stem Cells Dayt Ohio 37, 855–864

Aspden RM (2011): Obesity punches above its weight in osteoarthritis. Nat Rev Rheumatol 7, 65–68

Bachurski D, Schuldner M, Nguyen PH, Malz A, Reiners KS, Grenzi PC, Babatz F, Schauss AC, Hansen HP, Hallek M, Pogge von Strandmann E (2019): Extracellular vesicle measurements with nanoparticle tracking analysis - An accuracy and repeatability comparison between NanoSight NS300 and ZetaView. J Extracell Vesicles 8, 1596016

Bartel DP (2009): MicroRNAs: target recognition and regulatory functions. Cell 136, 215–233

Bayliss LE, Culliford D, Monk AP, Glyn Jones S, Judge A, Cooper C, Carr AJ, Arden NK, Beard DJ, Price AJ (2017): The effect of patient age at intervention on risk of implant revision after total replacement of the hip or knee: a population-based cohort study. Lancet 389, 1424–1430

Bengoa-Vergniory N, Kypta RM (2015): Canonical and noncanonical Wnt signaling in neural stem/progenitor cells. Cell Mol Life Sci 72, 4157–4172

Bernstein P, Sticht C, Jacobi A, Liebers C, Manthey S, Stiehler M (2010): Expression pattern differences between osteoarthritic chondrocytes and mesenchymal stem cells during chondrogenic differentiation. Osteoarthritis Cartilage 18, 1596–1607

Bertoli G, Cava C, Castiglioni I (2015): MicroRNAs: New Biomarkers for Diagnosis, Prognosis, Therapy Prediction and Therapeutic Tools for Breast Cancer. Theranostics 5, 1122–1143

Bettermann H, Cysarz D, Portsteffen A, Kümmell HC (2001): Bimodal dose-dependent effect on autonomic, cardiac control after oral administration of Atropa belladonna. Auton Neurosci 90, 132–137

Biniecka M, Kennedy A, Fearon U, Ng CT, Veale DJ, O'Sullivan JN (2010): Oxidative damage in synovial tissue is associated with in vivo hypoxic status in the arthritic joint. Ann Rheum Dis 69, 1172–1178

Boskey AL, Wians FH, Hauschka PV (1985): The effect of osteocalcin on in vitro lipid-induced hydroxyapatite formation and seeded hydroxyapatite growth. Calcif Tissue Int 37, 57–62

Botter SM, van Osch GJVM, Clockaerts S, Waarsing JH, Weinans H, van Leeuwen JPTM (2011): Osteoarthritis induction leads to early and temporal subchondral plate porosity in the tibial plateau of mice: an in vivo microfocal computed tomography study. Arthritis Rheum 63, 2690–2699

Chen CG, Thuillier D, Chin EN, Alliston T (2012): Chondrocyte-intrinsic Smad3 represses Runx2-inducible matrix metalloproteinase 13 expression to maintain articular cartilage and prevent osteoarthritis. Arthritis Rheum 64, 3278–3289

Reference

Chen W, Hill H, Christie A, Kim MS, Holloman E, Pavia-Jimenez A, Homayoun F, Ma Y, Patel N, Yell P, et al. (2016): Targeting renal cell carcinoma with a HIF-2 antagonist. Nature 539, 112–117

Chen Y, Zhao B, Zhu Y, Zhao H, Ma C (2019): HIF-1-VEGF-Notch mediates angiogenesis in temporomandibular joint osteoarthritis. Am J Transl Res 11, 2969–2982

Chern CM, Zhou H, Wang YH, Chang CL, Chiou WF, Chang WT, Yao CH, Liou KT, Shen YC (2020): Osthole ameliorates cartilage degradation by downregulation of NF-κB and HIF-2α pathways in an osteoarthritis murine model. Eur J Pharmacol 867, 172799

Chernyshev VS, Rachamadugu R, Tseng YH, Belnap DM, Jia Y, Branch KJ, Butterfield AE, Pease LF, Bernard PS, Skliar M (2015): Size and shape characterization of hydrated and desiccated exosomes. Anal Bioanal Chem 407, 3285–3301

Chu CR, Szczodry M, Bruno S (2010): Animal models for cartilage regeneration and repair. Tissue Eng Part B Rev 16, 105–115

Cizmar P, Yuana Y (2017): Detection and Characterization of Extracellular Vesicles by Transmission and Cryo-Transmission Electron Microscopy. Methods Mol Biol Clifton NJ 1660, 221–232

Clayton A, Court J, Navabi H, Adams M, Mason MD, Hobot JA, Newman GR, Jasani B (2001): Analysis of antigen presenting cell derived exosomes, based on immuno-magnetic isolation and flow cytometry. J Immunol Methods 247, 163–174

Coimbra IB, Jimenez SA, Hawkins DF, Piera-Velazquez S, Stokes DG (2004): Hypoxia inducible factor-1 alpha expression in human normal and osteoarthritic chondrocytes1. Osteoarthritis Cartilage 12, 336–345

Colombo M, Raposo G, Théry C (2014): Biogenesis, secretion, and intercellular interactions of exosomes and other extracellular vesicles. Annu Rev Cell Dev Biol 30, 255–289

Conde-Vancells J, Rodriguez-Suarez E, Embade N, Gil D, Matthiesen R, Valle M, Elortza F, Lu SC, Mato JM, Falcon-Perez JM (2008): Characterization and comprehensive proteome profiling of exosomes secreted by hepatocytes. J Proteome Res 7, 5157–5166

Cross M, Smith E, Hoy D, Nolte S, Ackerman I, Fransen M, Bridgett L, Williams S, Guillemin F, Hill CL, et al. (2014): The global burden of hip and knee osteoarthritis: estimates from the global burden of disease 2010 study. Ann Rheum Dis 73, 1323–1330

Dong Y-F, Soung DY, Schwarz EM, O'Keefe RJ, Drissi H (2006): Wnt induction of chondrocyte hypertrophy through the Runx2 transcription factor. J Cell Physiol 208, 77–86

Dunn W, DuRaine G, Reddi AH (2009): Profiling microRNA expression in bovine articular cartilage and implications for mechanotransduction. Arthritis Rheum 60, 2333–2339

Eijken M, Koedam M, van Driel M, Buurman CJ, Pols H a. P, van Leeuwen JPTM (2006): The essential role of glucocorticoids for proper human osteoblast differentiation and matrix mineralization. Mol Cell Endocrinol 248, 87–93

Endisha H, Rockel J, Jurisica I, Kapoor M (2018): The complex landscape of microRNAs in articular cartilage: biology, pathology, and therapeutic targets. JCI Insight 3, e121630

Epple LM, Griffiths SG, Dechkovskaia AM, Dusto NL, White J, Ouellette RJ, Anchordoquy TJ, Bemis LT, Graner MW (2012): Medulloblastoma exosome proteomics yield functional roles for extracellular vesicles. PloS One 7, e42064

Reference

Fitzner D, Schnaars M, Rossum D van, Krishnamoorthy G, Dibaj P, Bakhti M, Regen T, Hanisch U-K, Simons M (2011): Selective transfer of exosomes from oligodendrocytes to microglia by macropinocytosis. J Cell Sci 124, 447–458

Friedman RC, Farh KK-H, Burge CB, Bartel DP (2009): Most mammalian mRNAs are conserved targets of microRNAs. Genome Res 19, 92–105

Fu B, Wang Y, Zhang Xiali, Lang B, Zhou X, Xu X, Zeng T, Liu W, Zhang Xu, Guo J, Wang G (2015): MiR-221-induced PUMA silencing mediates immune evasion of bladder cancer cells. Int J Oncol 46, 1169–1180

Gan R, Yang Y, Yang X, Zhao L, Lu J, Meng QH (2014): Downregulation of miR-221/222 enhances sensitivity of breast cancer cells to tamoxifen through upregulation of TIMP3. Cancer Gene Ther 21, 290–296

GBD 2017 Disease and Injury Incidence and Prevalence Collaborators (2018): Global, regional, and national incidence, prevalence, and years lived with disability for 354 diseases and injuries for 195 countries and territories, 1990-2017: a systematic analysis for the Global Burden of Disease Study 2017. Lancet Lond Engl 392, 1789–1858

Giatromanolaki A, Sivridis E, Maltezos E, Athanassou N, Papazoglou D, Gatter KC, Harris AL, Koukourakis MI (2003): Upregulated hypoxia inducible factor-1alpha and -2alpha pathway in rheumatoid arthritis and osteoarthritis. Arthritis Res Ther 5, R193-201

Goldring MB (2005): Human chondrocyte cultures as models of cartilage-specific gene regulation. Methods Mol Med 107, 69–95

Gould SJ, Raposo G (2013): As we wait: coping with an imperfect nomenclature for extracellular vesicles. J Extracell Vesicles 2, eCollection 2013

Griffin TM, Scanzello CR (2019): Innate inflammation and synovial macrophages in osteoarthritis pathophysiology. Clin Exp Rheumatol 37 Suppl 120, 57–63

Hecht N, Johnstone B, Angele P, Walker T, Richter W (2019): Mechanosensitive MiRs regulated by anabolic and catabolic loading of human cartilage. Osteoarthritis Cartilage 27, 1208–1218

Heijink A, Gomoll AH, Madry H, Drobnič M, Filardo G, Espregueira-Mendes J, Van Dijk CN (2012): Biomechanical considerations in the pathogenesis of osteoarthritis of the knee. Knee Surg Sports Traumatol Arthrosc Off J ESSKA 20, 423–435

Hu X-H, Zhao Z-X, Dai J, Geng D-C, Xu Y-Z (2019): MicroRNA-221 regulates osteosarcoma cell proliferation, apoptosis, migration, and invasion by targeting CDKN1B/p27. J Cell Biochem 120, 4665–4674

Hunter DJ, Bierma-Zeinstra S (2019): Osteoarthritis. The Lancet 393, 1745–1759

Hurley M, Dickson K, Hallett R, Grant R, Hauari H, Walsh N, Stansfield C, Oliver S (2018): Exercise interventions and patient beliefs for people with hip, knee or hip and knee osteoarthritis: a mixed methods review. Cochrane Database Syst Rev 4, CD010842

Hwang HS, Park SJ, Lee MH, Kim HA (2017): MicroRNA-365 regulates IL-1β-induced catabolic factor expression by targeting HIF-2α in primary chondrocytes. Sci Rep 7, 17889

Iijima H, Aoyama T, Tajino J, Ito A, Nagai M, Yamaguchi S, Zhang X, Kiyan W, Kuroki H (2016): Subchondral plate porosity colocalizes with the point of mechanical load during ambulation in a rat knee model of post-traumatic osteoarthritis. Osteoarthritis Cartilage 24, 354–363

Reference

Iu M-F, Kaji H, Sowa H, Naito J, Sugimoto T, Chihara K (2005): Dexamethasone suppresses Smad3 pathway in osteoblastic cells. J Endocrinol 185, 131–138

Jing Q, Huang S, Guth S, Zarubin T, Motoyama A, Chen J, Padova FD, Lin S-C, Gram H, Han J (2005): Involvement of MicroRNA in AU-Rich Element-Mediated mRNA Instability. Cell 120, 623–634

Kamekura S, Hoshi K, Shimoaka T, Chung U, Chikuda H, Yamada T, Uchida M, Ogata N, Seichi A, Nakamura K, Kawaguchi H (2005): Osteoarthritis development in novel experimental mouse models induced by knee joint instability. Osteoarthritis Cartilage 13, 632–641

Kamekura S, Kawasaki Y, Hoshi K, Shimoaka T, Chikuda H, Maruyama Z, Komori T, Sato S, Takeda S, Karsenty G, et al. (2006): Contribution of runt-related transcription factor 2 to the pathogenesis of osteoarthritis in mice after induction of knee joint instability. Arthritis Rheum 54, 2462–2470

Karim A, Amin AK, Hall AC (2018): The clustering and morphology of chondrocytes in normal and mildly degenerate human femoral head cartilage studied by confocal laser scanning microscopy. J Anat 232, 686–698

Kiaer T, Grønlund J, Sørensen KH (1988): Subchondral pO2, pCO2, pressure, pH, and lactate in human osteoarthritis of the hip. Clin Orthop 149–155

Kolasinski SL, Neogi T, Hochberg MC, Oatis C, Guyatt G, Block J, Callahan L, Copenhaver C, Dodge C, Felson D, et al. (2020): 2019 American College of Rheumatology/Arthritis Foundation Guideline for the Management of Osteoarthritis of the Hand, Hip, and Knee. Arthritis Care Res 72, 149–162

Komori T (2018): Runx2, an inducer of osteoblast and chondrocyte differentiation. Histochem Cell Biol 149, 313–323

Krishnasamy P, Hall M, Robbins SR (2018): The role of skeletal muscle in the pathophysiology and management of knee osteoarthritis. Rheumatology 57, 22–33

Krock BL, Eisinger-Mathason TS, Giannoukos DN, Shay JE, Gohil M, Lee DS, Nakazawa MS, Sesen J, Skuli N, Simon MC (2015): The aryl hydrocarbon receptor nuclear translocator is an essential regulator of murine hematopoietic stem cell viability. Blood 125, 3263–3272

Lee RC, Feinbaum RL, Ambros V (1993): The C. elegans heterochronic gene lin-4 encodes small RNAs with antisense complementarity to lin-14. Cell 75, 843–854

Lee Y, Kim M, Han J, Yeom K-H, Lee S, Baek SH, Kim VN (2004): MicroRNA genes are transcribed by RNA polymerase II. EMBO J 23, 4051–4060

Leopoldino AO, Machado GC, Ferreira PH, Pinheiro MB, Day R, McLachlan AJ, Hunter DJ, Ferreira ML (2019): Paracetamol versus placebo for knee and hip osteoarthritis. Cochrane Database Syst Rev 2, CD013273

Levick JR (1990): Hypoxia and acidosis in chronic inflammatory arthritis; relation to vascular supply and dynamic effusion pressure. J Rheumatol 17, 579–582

Lim LP, Lau NC, Garrett-Engele P, Grimson A, Schelter JM, Castle J, Bartel DP, Linsley PS, Johnson JM (2005): Microarray analysis shows that some microRNAs downregulate large numbers of target mRNAs. Nature 433, 769–773

Reference

Liu B, Lu Y, Wang Y, Ge L, Zhai N, Han J (2019): A protocol for isolation and identification and comparative characterization of primary osteoblasts from mouse and rat calvaria. Cell Tissue Bank 20, 173–182

Liu S, Wang Z, Liu Z, Shi S, Zhang Z, Zhang J, Lin H (2018): miR-221/222 activate the Wnt/β-catenin signaling to promote triple-negative breast cancer. J Mol Cell Biol 10, 302–315

Lo Cicero A, Stahl PD, Raposo G (2015): Extracellular vesicles shuffling intercellular messages: for good or for bad. Curr Opin Cell Biol 35, 69–77

Loeser RF, Goldring SR, Scanzello CR, Goldring MB (2012): Osteoarthritis: a disease of the joint as an organ. Arthritis Rheum 64, 1697–1707

Lolli A, Lambertini E, Penolazzi L, Angelozzi M, Morganti C, Franceschetti T, Pelucchi S, Gambari R, Piva R (2014): Pro-chondrogenic effect of miR-221 and slug depletion in human MSCs. Stem Cell Rev Rep 10, 841–855

Lötvall J, Hill AF, Hochberg F, Buzás EI, Vizio DD, Gardiner C, Gho YS, Kurochkin IV, Mathivanan S, Quesenberry P, et al. (2014): Minimal experimental requirements for definition of extracellular vesicles and their functions: a position statement from the International Society for Extracellular Vesicles. J Extracell Vesicles 3, 26913

Lund E, Dahlberg JE (2006): Substrate selectivity of exportin 5 and Dicer in the biogenesis of microRNAs. Cold Spring Harb Symp Quant Biol 71, 59–66

Madry H, Kon E, Condello V, Peretti GM, Steinwachs M, Seil R, Berruto M, Engebretsen L, Filardo G, Angele P (2016): Early osteoarthritis of the knee. Knee Surg Sports Traumatol Arthrosc Off J ESSKA 24, 1753–1762

Mandl M, Depping R (2014): Hypoxia-Inducible Aryl Hydrocarbon Receptor Nuclear Translocator (ARNT) (HIF-1β): Is It a Rare Exception? Mol Med 20, 215–220

Marlovits S, Hombauer M, Truppe M, Vècsei V, Schlegel W (2004): Changes in the ratio of type-I and type-II collagen expression during monolayer culture of human chondrocytes. J Bone Joint Surg Br 86, 286–295

Mause SF, Weber C (2010): Microparticles: protagonists of a novel communication network for intercellular information exchange. Circ Res 107, 1047–1057

McAlindon TE, LaValley MP, Harvey WF, Price LL, Driban JB, Zhang M, Ward RJ (2017): Effect of Intra-articular Triamcinolone vs Saline on Knee Cartilage Volume and Pain in Patients With Knee Osteoarthritis: A Randomized Clinical Trial. JAMA 317, 1967–1975

Medina R, Zaidi SK, Liu C-G, Stein JL, van Wijnen AJ, Croce CM, Stein GS (2008): MicroRNAs 221 and 222 bypass quiescence and compromise cell survival. Cancer Res 68, 2773–2780

Mikami Y, Omoteyama K, Kato S, Takagi M (2007): Inductive effects of dexamethasone on the mineralization and the osteoblastic gene expressions in mature osteoblast-like ROS17/2.8 cells. Biochem Biophys Res Commun 362, 368–373

Minciacchi VR, Freeman MR, Di Vizio D (2015): Extracellular vesicles in cancer: exosomes, microvesicles and the emerging role of large oncosomes. Semin Cell Dev Biol 40, 41–51

Mizrak A, Bolukbasi MF, Ozdener GB, Brenner GJ, Madlener S, Erkan EP, Ströbel T, Breakefield XO, Saydam O (2013): Genetically engineered microvesicles carrying suicide mRNA/protein inhibit schwannoma tumor growth. Mol Ther J Am Soc Gene Ther 21, 101–108

Reference

Mora JC, Przkora R, Cruz-Almeida Y (2018): Knee osteoarthritis: pathophysiology and current treatment modalities. J Pain Res 11, 2189–2196

Muhammad SA, Nordin N, Hussin P, Mehat MZ, Tan SW, Fakurazi S (2019): Optimization of Protocol for Isolation of Chondrocytes from Human Articular Cartilage. CARTILAGE 3, 872S-884S

Murchison EP, Hannon GJ (2004): miRNAs on the move: miRNA biogenesis and the RNAi machinery. Curr Opin Cell Biol 16, 223–229

Murphy LB, Cisternas MG, Pasta DJ, Helmick CG, Yelin EH (2018): Medical Expenditures and Earnings Losses Among US Adults With Arthritis in 2013. Arthritis Care Res 70, 869–876

Nakamura H, Vo P, Kanakis I, Liu K, Bou-Gharios G (2020): Aggrecanase-selective tissue inhibitor of metalloproteinase-3 (TIMP3) protects articular cartilage in a surgical mouse model of osteoarthritis. Sci Rep 10, 1–9

Nelson AE (2018): Osteoarthritis year in review 2017: clinical. Osteoarthritis Cartilage 26, 319–325

Nelson AE, Allen KD, Golightly YM, Goode AP, Jordan JM (2014): A systematic review of recommendations and guidelines for the management of osteoarthritis: The Chronic Osteoarthritis Management Initiative of the U.S. Bone and Joint Initiative. Semin Arthritis Rheum 43, 701–712

O'Connor MI (2006): Osteoarthritis of the hip and knee: sex and gender differences. Orthop Clin North Am 37, 559–568

Pan B-T, Johnstone RM (1983): Fate of the transferrin receptor during maturation of sheep reticulocytes in vitro: Selective externalization of the receptor. Cell 33, 967–978

Pan J, Zhou X, Li W, Novotny JE, Doty SB, Wang L (2009): In situ measurement of transport between subchondral bone and articular cartilage. J Orthop Res Off Publ Orthop Res Soc 27, 1347–1352

Pan J-M, Wu L-G, Cai J-W, Wu L-T, Liang M (2019): Dexamethasone suppresses osteogenesis of osteoblast via the PI3K/Akt signaling pathway in vitro and in vivo. J Recept Signal Transduct Res 39, 80–86

Pegtel DM, Gould SJ (2019): Exosomes. Annu Rev Biochem 88, 487–514

Pfander D, Gelse K (2007): Hypoxia and osteoarthritis: how chondrocytes survive hypoxic environments. Curr Opin Rheumatol 19, 457–462

Poulet B, Liu K, Plumb D, Vo P, Shah M, Staines K, Sampson A, Nakamura H, Nagase H, Carriero A, et al. (2016): Overexpression of TIMP-3 in Chondrocytes Produces Transient Reduction in Growth Plate Length but Permanently Reduces Adult Bone Quality and Quantity. PloS One 11, e0167971

Qi JH, Anand-Apte B (2015): Tissue Inhibitor of Metalloproteinase-3 (TIMP3) Promotes Endothelial Apoptosis via a Caspase-Independent Mechanism. Apoptosis Int J Program Cell Death 20, 523–534

Qing L, Lei P, Liu H, Xie J, Wang L, Wen T, Hu Y (2017): Expression of hypoxia-inducible factor-1α in synovial fluid and articular cartilage is associated with disease severity in knee osteoarthritis. Exp Ther Med 13, 63–68

Reference

Rahmati M, Nalesso G, Mobasheri A, Mozafari M (2017): Aging and osteoarthritis: Central role of the extracellular matrix. Ageing Res Rev 40, 20–30

Ramasubbu K, Gurm H, Litaker D (2001): Gender bias in clinical trials: do double standards still apply? J Womens Health Gend Based Med 10, 757–764

Rana TM (2007): Illuminating the silence: understanding the structure and function of small RNAs. Nat Rev Mol Cell Biol 8, 23–36

Regev-Rudzki N, Wilson DW, Carvalho TG, Sisquella X, Coleman BM, Rug M, Bursac D, Angrisano F, Gee M, Hill AF, et al. (2013): Cell-Cell Communication between Malaria-Infected Red Blood Cells via Exosome-like Vesicles. Cell 153, 1120–1133

Rice SJ, Beier F, Young DA, Loughlin J (2020): Interplay between genetics and epigenetics in osteoarthritis. Nat Rev Rheumatol 16, 268–281

Riffo-Campos ÁL, Riquelme I, Brebi-Mieville P (2016): Tools for Sequence-Based miRNA Target Prediction: What to Choose? Int J Mol Sci 17, 1987

Rothrauff BB, Jorge A, de Sa D, Kay J, Fu FH, Musahl V (2020): Anatomic ACL reconstruction reduces risk of post-traumatic osteoarthritis: a systematic review with minimum 10-year follow-up. Knee Surg Sports Traumatol Arthrosc 28, 1072–1084

Sanchez C, Deberg MA, Piccardi N, Msika P, Reginster J-YL, Henrotin YE (2005): Osteoblasts from the sclerotic subchondral bone downregulate aggrecan but upregulate metalloproteinases expression by chondrocytes. This effect is mimicked by interleukin-6, -1β and oncostatin M pre-treated non-sclerotic osteoblasts. Osteoarthritis Cartilage 13, 979–987

Schmid CL, Kennedy NM, Ross NC, Lovell KM, Yue Z, Morgenweck J, Cameron MD, Bannister TD, Bohn LM (2017): Bias Factor and Therapeutic Window Correlate to Predict Safer Opioid Analgesics. Cell 171, 1165–1175

Seibel MJ, Cooper MS, Zhou H (2013): Glucocorticoid-induced osteoporosis: mechanisms, management, and future perspectives. Lancet Diabetes Endocrinol 1, 59–70

Shalhoub V, Conlon D, Tassinari M, Quinn C, Partridge N, Stein GS, Lian JB (1992): Glucocorticoids promote development of the osteoblast phenotype by selectively modulating expression of cell growth and differentiation associated genes. J Cell Biochem 50, 425–440

Song Q, An Q, Niu B, Lu X, Zhang N, Cao X (2019): Role of miR-221/222 in Tumor Development and the Underlying Mechanism. J Oncol 2019, 7252013

Spitaels D, Mamouris P, Vaes B, Smeets M, Luyten F, Hermens R, Vankrunkelsven P (2020): Epidemiology of knee osteoarthritis in general practice: a registry-based study. BMJ Open 10, e031734

Stadnik PS, Gilbert SJ, Tarn J, Charlton S, Skelton AJ, Barter MJ, Duance VC, Young DA, Blain EJ (2021): Regulation of microRNA-221, -222, -21 and -27 in articular cartilage subjected to abnormal compressive forces. J Physiol 599, 143–155

Sverdlov ED (2012): Amedeo Avogadro's cry: what is 1 μg of exosomes? BioEssays News Rev Mol Cell Dev Biol 34, 873–875

Tachmazidou I, Hatzikotoulas K, Southam L, Esparza-Gordillo J, Haberland V, Zheng J, Johnson T, Koprulu M, Zengini E, Steinberg J, et al. (2019): Identification of new therapeutic

targets for osteoarthritis through genome-wide analyses of UK Biobank data. Nat Genet 51, 230–236

Taheri S, Winkler T, Schenk LS, Neuerburg C, Baumbach SF, Zustin J, Lehmann W, Schilling AF (2019): Developmental Transformation and Reduction of Connective Cavities within the Subchondral Bone. Int J Mol Sci 20, 770

Taheri S, Yoshida T, Böker KO, Foerster RH, Jochim L, Flux AL, Grosskopf B, Lehmann W, Schilling AF (2021): Investigating the Microchannel Architectures Inside the Subchondral Bone in Relation to Estimated Hip Reaction Forces on the Human Femoral Head. Calcif Tissue Int 1, 510–524

Tauro BJ, Greening DW, Mathias RA, Ji H, Mathivanan S, Scott AM, Simpson RJ (2012): Comparison of ultracentrifugation, density gradient separation, and immunoaffinity capture methods for isolating human colon cancer cell line LIM1863-derived exosomes. Methods San Diego Calif 56, 293–304

Théry C, Boussac M, Véron P, Ricciardi-Castagnoli P, Raposo G, Garin J, Amigorena S (2001): Proteomic Analysis of Dendritic Cell-Derived Exosomes: A Secreted Subcellular Compartment Distinct from Apoptotic Vesicles. J Immunol 166, 7309–7318

Théry C, Amigorena S, Raposo G, Clayton A (2006): Isolation and characterization of exosomes from cell culture supernatants and biological fluids. Curr Protoc Cell Biol Chapter 3, Unit 3.22

Théry C, Witwer KW, Aikawa E, Alcaraz MJ, Anderson JD, Andriantsitohaina R, Antoniou A, Arab T, Archer F, Atkin-Smith GK, et al. (2018): Minimal information for studies of extracellular vesicles 2018 (MISEV2018): a position statement of the International Society for Extracellular Vesicles and update of the MISEV2014 guidelines. J Extracell Vesicles 7, 1535750

Tkach M, Théry C (2016): Communication by Extracellular Vesicles: Where We Are and Where We Need to Go. Cell 164, 1226–1232

Tkach M, Kowal J, Théry C (2018): Why the need and how to approach the functional diversity of extracellular vesicles. Philos Trans R Soc Lond B Biol Sci 373, 20160479

Treuhaft PS, MCCarty DJ (1971): Synovial fluid pH, lactate, oxygen and carbon dioxide partial pressure in various joint diseases. Arthritis Rheum 14, 475–484

Urban H, Little CB (2018): The role of fat and inflammation in the pathogenesis and management of osteoarthritis. Rheumatology 57, 10–21

Valadi H, Ekström K, Bossios A, Sjöstrand M, Lee JJ, Lötvall JO (2007): Exosome-mediated transfer of mRNAs and microRNAs is a novel mechanism of genetic exchange between cells. Nat Cell Biol 9, 654–659

van der Voet JA, Runhaar J, van der Plas P, Vroegindeweij D, Oei EH, Bierma-Zeinstra SMA (2017): Baseline meniscal extrusion associated with incident knee osteoarthritis after 30 months in overweight and obese women. Osteoarthritis Cartilage 25, 1299–1303

Vos T, Flaxman AD, Naghavi M, Lozano R, Michaud C, Ezzati M, Shibuya K, Salomon JA, Abdalla S, Aboyans V, et al. (2012): Years lived with disability (YLDs) for 1160 sequelae of 289 diseases and injuries 1990-2010: a systematic analysis for the Global Burden of Disease Study 2010. Lancet Lond Engl 380, 2163–2196

Reference

Wang GL, Jiang BH, Rue EA, Semenza GL (1995): Hypoxia-inducible factor 1 is a basic-helix-loop-helix-PAS heterodimer regulated by cellular O2 tension. Proc Natl Acad Sci U S A 92, 5510–5514

Wang P, Mao Z, Pan Q, Lu R, Huang X, Shang X, Zhang R, You H (2018): Histone deacetylase-4 and histone deacetylase-8 regulate interleukin-1β-induced cartilage catabolic degradation through MAPK/JNK and ERK pathways. Int J Mol Med 41, 2117–2127

Wang R, Jiang W, Zhang L, Xie S, Zhang S, Yuan S, Jin Y, Zhou G (2020): Intra-articular delivery of extracellular vesicles secreted by chondrogenic progenitor cells from MRL/MpJ superhealer mice enhances articular cartilage repair in a mouse injury model. Stem Cell Res Ther 11, 93

Wang Y, Fan X, Xing L, Tian F (2019): Wnt signaling: a promising target for osteoarthritis therapy. Cell Commun Signal CCS 17, 97

Yáñez-Mó M, Siljander PR-M, Andreu Z, Zavec AB, Borràs FE, Buzas EI, Buzas K, Casal E, Cappello F, Carvalho J, et al. (2015): Biological properties of extracellular vesicles and their physiological functions. J Extracell Vesicles 4, 27066

Yelin E, Murphy L, Cisternas MG, Foreman AJ, Pasta DJ, Helmick CG (2007): Medical Care Expenditures and Earnings Losses Among Persons With Arthritis and Other Rheumatic Conditions in 2003, and Comparisons With 1997. Arthritis Rheum 56, 1397–1407

Yuan Q, Loya K, Rani B, Möbus S, Balakrishnan A, Lamle J, Cathomen T, Vogel A, Manns MP, Ott M, et al. (2013): MicroRNA-221 overexpression accelerates hepatocyte proliferation during liver regeneration. Hepatol Baltim Md 57, 299–310

Zeng C, Wei J, Persson MSM, Sarmanova A, Doherty M, Xie D, Wang Y, Li X, Li J, Long H, et al. (2018): Relative efficacy and safety of topical non-steroidal anti-inflammatory drugs for osteoarthritis: a systematic review and network meta-analysis of randomised controlled trials and observational studies. Br J Sports Med 52, 642–650

Zengini E, Hatzikotoulas K, Tachmazidou I, Steinberg J, Hartwig FP, Southam L, Hackinger S, Boer CG, Styrkarsdottir U, Gilly A, et al. (2018): Genome-wide analyses using UK Biobank data provide insights into the genetic architecture of osteoarthritis. Nat Genet 50, 549–558

Zhang W, Peng F, Zhou T, Huang Y, Zhang L, Ye P, Lu M, Yang G, Gai Y, Yang T, et al. (2015): Targeted delivery of chemically modified anti-miR-221 to hepatocellular carcinoma with negatively charged liposomes. Int J Nanomedicine 10, 4825–4836

Zhang Y, Gao Y, Cai L, Li F, Lou Y, Xu N, Kang Y, Yang H (2017): MicroRNA-221 is involved in the regulation of osteoporosis through regulates RUNX2 protein expression and osteoblast differentiation. Am J Transl Res 9, 126–135

Zhen G, Cao X (2014): Targeting TGFβ signaling in subchondral bone and articular cartilage homeostasis. Trends Pharmacol Sci 35, 227–236

Zheng X, Zhao F-C, Pang Y, Li D-Y, Yao S-C, Sun S-S, Guo K-J (2017): Downregulation of miR-221-3p contributes to IL-1β-induced cartilage degradation by directly targeting the SDF1/CXCR4 signaling pathway. J Mol Med Berl Ger 95, 615–627

Zhou X, Ruan J, Wang G, Zhang W (2007): Characterization and Identification of MicroRNA Core Promoters in Four Model Species. PLoS Comput Biol 3, 0412–0423

Zhou Y, Wang T, Hamilton JL, Chen D (2017): Wnt/β-catenin Signaling in Osteoarthritis and in Other Forms of Arthritis. Curr Rheumatol Rep 19, 53

FUNDING RELATED TO THIS THESIS

This study was supported by a scholarship from the China Scholarship Council [No. 202008080030].

ACKNOWLEDGEMENTS

First of all, I would like to express my deepest gratitude to my supervisor Prof. Arndt F. Schilling for providing this precious opportunity to study here. Thank you for your patient guidance and 100% support during my research in Göttingen. More importantly, it's your meritorious encouragement, thoughtful kindness and shining advice that promoted me to overcome difficulties in my study.

I would like to express my sincere gratitude to my second supervisor Prof. Nicolai Miosge, for his continuous support in my work. When there were difficulties, he always gave amazing suggestions and guides.

I would like to thank Prof. Hongbo You, Prof. Zhengqiang Luo, Prof. Ziyang Zhang, and Prof. Tao Fu for their great help, encouragement, guidance during my application to study at UMG. Without their help, I would not be here.

I would like to thank Dr. Kai Böker for his patient and unselfish guidance, support, and helpful discussions. Whenever I needed his help, he was always there. Thanks to your company in the lab for nearly three years, I feel less lonely.

I would like to thank Ramona Castro Machguth, Kathrin Hannke, Dr. Shahed Taheri, Samuel Siegk, Joachim Wagner, Michel Remling, Eyck Rodenwaldt. Many thanks to all the teammates who helped me with my study and life here.

Furthermore, a special thank goes to Swetlana Sperling and Dr. Milena Ninkovic for their kind and warm help in my daily life.

Thanks for everything!

CURRICULUM VITAE

My name is Xiaobin Shang, male, born on 29th September 1991 in Shangqiu of Henan province in China. I got my bachelor's degree in Clinical Medicine (Human) from Xinxiang Medical College from September 2009 to July 2014 and got my master's degree in Surgery (Orthopedics) from Huazhong University of Science and Technology from September 2014 to July 2017. During 8 years of medical education in China, I spent 3 years in clinical practice in Tongji hospital in Wuhan and passed the national exam for the Chinese medical board in 2015. From July 2017 to June 2019, I was employed by Wuhan Tongren Hospital as an orthopedic surgeon. Since July 2019, I started a medical doctorate study in the department of trauma orthopedic and plastic surgery at Georg August University Medical Center Göttingen with the support of a scholarship from the China Scholarship Council.